

47 *it be best to minimize the plumbing and/or detection delays using a system with a much faster*
48 *response time? E.g. use of 1/8" tubing, CO₂ gas, and LICOR CO₂ detector could achieve response*
49 *times of probably only a few seconds, couldn't it? It would be useful to discuss/recommend the*
50 *best experimental practices to most easily and accurately extract the parameters that other OFR*
51 *users could then apply to their systems, based on what was learned in this study.*

52
53 The referee offers a fair, thought-provoking argument. On one hand, an alternate method
54 to minimize plumbing and increase response time may minimize bias in the results
55 (although can still be present). On the other hand, our method entirely removes operation-
56 specific bias, and is conveniently adaptable to multiple inlets and outlets, or any other
57 operation-specific arrangement that may be required given other constraints. We believe
58 there are multiple scenarios in which minimizing plumbing and utilizing on-hand
59 instrumentation, such as the LI-COR LI-820 CO₂ Analyzer, may not be feasible or cost-
60 effective. For example, there can be physical/space limitations as to how short plumbing
61 lines can be, there may be a need for peripheral inlets and outlets (e.g., "cNO" idealized
62 configuration in (Peng et al., 2017)) or requirements for additional dilutors, scrubbers, etc.,
63

64 Also, novel techniques strive to minimize residence time in OFRs (e.g., Simonen et al.,
65 2016). It is arguable if in exceedingly large OFRs, such as the CPOT (Huang et al., 2016),
66 the spacetime in the lines is so small that any RTD in the plumbing will not affect the
67 overall RTD. However this assumption loses validity as the spacetimes of the tubing and
68 reactor become comparable or non-negligible. The RTD should only apply for fluid
69 moving in the reaction zone – and for OFRs the reaction zone is confined to the zone
70 illuminated by the UV lamps (the OFR itself). Our method also allows for data correction
71 post-experiment, if necessary. While we are hesitant to offer best practice
72 recommendations without quantitative data, we have included the following (lines 454-461
73 of the revised manuscript):

74
75 "We do recognize that OFR (or any environmental chemical reactor) users may have a
76 preference to rapidly obtain an RTD profile perhaps using an improvised setup with very
77 short sample lines and a fast time-response gas analyzer. However, the accuracy to which
78 the profile is obtained should be carefully examined. If the reactor is considerably large, or
79 if it is an OFR to be deployed for low levels of exposure, then the influence of plumbing is
80 minimal. If the reactor of choice is small, the oxidant exposure is high, or the reactor has
81 more than one inlet/outlet or other peripheral components, it would be recommended to
82 use the method described here to obtain the most representative RTD, since all sources of
83 bias are removed."

84
85 **[In reference to: Detailed Comments]**

86
87 - P5, L97: Ortega et al. 2015 should be updated to ACP 2016.

88
89 We have updated the citation from the discussion article to the final article.

90
91 - P5, L97-104 (and latter part of the intro such as P6, L126-128) seems to be missing some of the
92 recent literature related to measured/modeled RTDs and chemical effects in PAM-type OFRs that

93 would provide better context of what has/hasn't been done in terms of modeling/characterizing
94 OFR flow (especially PAM-type most relevant to this work). These include (but may not be limited
95 to): Peng et al. 2015 (which the authors cite earlier) expands substantially on the Li et al paper
96 and discusses how different flow RTD assumptions (plug, laminar, measured) affect OH exposure
97 (see Section 3.5, Figs. 9, 10, S11, S12, S16, Table S1); Ortega et al. ACP 2016 (cited elsewhere)
98 shows FLUENT CFDs of with/without the inlet plate installed (Section 2.2, Fig. S1); Palm et al.
99 ACP 2017 (www.atmos-chem-phys.net/17/5331/2017/) shows RTDs from FLUENT CFDs without
100 the inlet plate installed for the PAM OFR for different particles sizes and compared to the Lambe
101 et al 2011 RTD. (Section 2.2, Fig. S1); Palm et al. ACPD, 2017 (<https://doi.org/10.5194/acp-2017-795>) shows some modeled chemical differences (in VOC decays) for different RTD flow
102 assumptions (Figs. 1, 2, S6).
103

104
105 Similar to the first comment in the Main Comments section, we thank the reviewer for
106 highlighting this recent work. With reference to L102-112, we included the following in
107 place of the last sentence of the paragraph:
108

109 “Following an experimentally determined RTD (Lambe et al., 2011) in a PAM OFR, Peng
110 et al. extend the model developed by Li et al., to include this non-ideal RTD, suggesting
111 model disagreement at high exposures. Ortega et al. employ FLUENT to show that removal
112 of the inlet plate (resulting in a less pronounced aperture to the reactor) significantly
113 decreases recirculation regions; and Palm et al. then extend the simulation to show that the
114 FLUENT-derived RTD (Palm et al., 2017) has a narrower distribution than the
115 experimentally-derived RTD by Lambe et al. Finally, Peng and Jimenez lay an initial
116 framework for the possibility of OFRs investigating NO chemistry (Peng and Jimenez,
117 2017), where initial sensitivity analysis on RTDs suggest considerable model disagreement
118 at high exposures. The fundamental caveat in this recent work is the reliance on an
119 accurately determined experimental RTD, that provides the basis for error analysis.”
120

121 With respect to the latter part of the introduction (L126-128 of the original manuscript
122 pointed out by the referee), we believe to have reviewed the literature appropriately. The
123 intent of this paragraph was to compare experimental methods and experimentally-
124 obtained RTDs, such as those in Lambe et al (2011a), Huang et al. (2016), and Simonen et
125 al. (2016). Literature suggested by the referee employs FLUENT to either model an RTD
126 or takes the compartmental model from Lambe et al. (2011a) to interpret their results, but
127 does not provide an approach to experimentally obtaining RTDs, per se. To clarify this
128 point, the sentence (lines 134-136 in the revised manuscript) now reads:
129

130 “We compare this approach to that of previous studies by Lambe et al. (2011a), Huang et
131 al. (2016), and Simonen et al. (2016), which to the best of our knowledge are the only other
132 studies to date that report experimentally-derived RTDs in OFRs.”
133

134 Nonetheless, the review of the very recent literature indeed provided better context for our
135 introduction, for which we thank the reviewer as our manuscript is now significantly
136 improved.
137

138 - P7, L161: consider reporting SO2 tank concentration.

139
140
141
142
143
144
145
146
147
148
149
150
151
152
153
154
155
156
157
158
159
160
161
162
163
164
165
166
167
168
169
170
171
172
173
174
175
176
177
178
179
180
181
182
183
184

We added a note here that states 3 ppm SO₂ tank concentration.

- P8, L182: delete “create” or “allow”

Similar to Reviewer 2, we thank the referee for pointing this out, and have deleted “allow”.

- P10, L218: add hyphen for first-order

We changed “first order” to “first-order”.

- P10, L224-225: What is meant by “however those simulations required significant computer time to resolve mesh sizing”? Do the authors mean to say it would take too much time to run (or justify running) for this study?

Yes. We have deleted the ambiguous phrase, and added the new sentence below (lines 233-236 of the revised manuscript):

“However, resolving the simulation mesh size to account for these internals significantly extended the computational requirements, to the point that running these simulations was not possible on our computer system and would require a computing cluster to perform.”

- P18, L395-397: Again, more detailed modeling work from other publications on effects of differing RTDs and flow assumptions missing here.

We thank the referee for bringing this to our attention, and have included references from (Palm et al., 2017, 2018, Peng et al., 2015, 2016; Peng and Jimenez, 2017) in this section, with additional discussion suggested by Reviewer 2. We have restructured the paragraph (lines 406-434 in the revised manuscript):

“Initial PAM modeling work assumed plug flow behavior in OFRs (Li et al., 2015). Li et al. stated that correcting for the non-ideal E-Curve in their OFR would account for ~10% error in their oxidant exposure results, which is less than the overall model uncertainty. However, recent work incorporates the effect of non-ideal RTDs on model outputs (Palm et al., 2017, 2018, Peng et al., 2015, 2016; Peng and Jimenez, 2017). Peng et al. (2015) show that for three OFR operational modes (that is, modes of different oxidant formation mechanisms denoted by ‘OFR185’, ‘OFR254-70’, and ‘OFR254-7’), a comparison between model output for ideal plug flow vs. non-ideal RTDs (using the RTD experimentally obtained by Lambe et al., 2011a) for OH exposure (OH_{exp}) generally agree within a factor of 2 for low OH_{exp}; the model disagreement exacerbates at high OH_{exp} beyond a factor of ~4. Peng and Jimenez then extend OFR operational modes to include N-containing chemistry (in modes referred to therein as ‘OFR185-iNO’, ‘OFR185-7-iNO’, and ‘OFR185-70-iNO’) where at moderate-to-high OH_{exp}, the deviations exacerbate significantly, although the authors argue those conditions represent unrealistic chemical pathways. It is worthwhile noting that the chemistry modeled by Peng and Jimenez may find a workaround by utilizing N₂O as NO precursor (Lambe et al., 2017) rather than NO

185 itself, potentially minimizing RTD-related errors. Palm et al. (2018) report data from OFR
186 field deployment where the same comparison (ideal plug flow vs. the RTD experimentally
187 obtained by Lambe et al., 2011a) suggests RTD-related errors overpredict (for CO) or
188 underpredict (for toluene and monoterpenes) photochemical age (that is, the ratio of OH_{exp}
189 to tropospheric average OH number concentrations) in the reactor, generally within a factor
190 of 3 of model error. Considering this work employs the compartmental model RTD
191 described by Lambe et al. (2011a), which for reasons mentioned in the previous section
192 may not be the true PAM RTD, and given that non-ideality in RTDs affects certain OFRs
193 more than others, implementing the method presented here to obtain a more representative
194 reactor RTD can either help constrain error uncertainty in the models, or possibly extend
195 the OH_{exp} range in which OFRs can be operated, a reportedly nontrivial task (Palm et al.,
196 2018). Considering our results indicate that OFRs like the WU-PAM exhibit an RTD
197 closely matching that of an ideal CSTR, which is more well-mixed than the Lambe et al.
198 RTD, the sensitivity analysis conducted so far could represent a lower bound for error
199 analysis because the Lambe et al. RTD is closer to a PFR-like RTD than a CSTR-like
200 RTD.”

201
202 - P18-19: “Potential Implications” section. The use of OHR_{ext} appears to not be accurately used.
203 OHR is not an exclusively intensive property of a compound (as seems to be implied in the text)
204 but rather depends on the concentration and OH rate constants of the compounds present that can
205 react with OH. Also OHR is a measure of the (inverse) OH lifetime, not its reaction partners.
206 Maybe the authors really mean the OH lifetime of different compounds? i.e. $k_{\text{voc}+\text{oh}} \times [\text{OH}]$.

207
208 We replaced ‘OHR_{ext}’ with ‘lifetime to OH’ and restructured the paragraph (lines 436-451
209 in the revised manuscript):

210
211 “For compounds with low lifetimes to OH, contacting could influence the model results to
212 a greater extent (e.g., field deployment monoterpene decay reported by Palm et al., 2018).
213 By taking a ratio of characteristic reaction time to the characteristic transport time, one can
214 define the Damköhler number (Da_n). Considering spacetimes of 52-411 s (as per this study),
215 the value of Da_n can be between 0.52 and 4.11 for a compound with lifetimes of ~100s.
216 Since reaction timescales are on the order of transport timescales, contact patterns may
217 play an important role, as seen in Palm et al. (2018). This could also be the case for
218 heterogenous reactions, diffusion-limited reactions, or semivolatile compound (SVOC)
219 oxidation that exhibit slow gas-particle partitioning. Furthermore, combining a
220 phenomenological model to an associated RTD can impact kinetics (and yields) further.
221 The RTD generated by Lambe et al. (2011a) employed in Li et al. (2015) may lead to
222 greater than 10% error if the 2 PFRs in parallel model suggested by Lambe et al. (2011a)
223 is not applicable. In these scenarios, ensuring a high degree of plug flow can not only
224 maximize exposure, but minimize the distribution of aged compounds (e.g., first or second
225 generation compounds) that are due to different exit ages because of recirculation or
226 stagnation. However, this configuration may not suit a field deployment where trace
227 compounds have short lifetimes to OH and can be easily lost to reactor walls, in which case
228 ensuring a high degree of mixing would be beneficial.”
229

230 - P19, L412-16: *It's not clear why compounds that react faster with OH would be more prone to*
231 *be lost to the reactor walls. It seems that the opposite is stated above. Also not clear how rapid*
232 *mixing would help that situation.*

233
234 We removed this argument from our discussion.

235
236 - P19, L406-407. Add "a" before phenomenological or make "model" plural.

237
238 We incorporated "a" in the sentence:

239
240 "Furthermore, combining a phenomenological model to an associated RTD can impact
241 kinetics (and yields) further."

242
243 - P19, L412: Statement: *"This configuration would suit a laboratory experiment with slow kinetics,*
244 *where concentrations can be made high enough to where wall losses aren't an issue."* This
245 *statement may be very misleading. Simply increasing concentrations in many cases does not*
246 *decrease the relative importance of wall effects since they are often first-order losses and the walls*
247 *may not necessarily establish equilibrium and relevant timescales. Please revise to precisely state*
248 *what is meant here, or possibly delete if not relevant.*

249
250 Upon re-examination of the sentence, we removed the sentence altogether.

251
252 - P20, L442: add "the" or "a" before "focus"

253
254 We incorporated "a" in the sentence:

255
256 "Finally, to obtain accurate experimental RTDs, achieving a functional direct
257 deconvolution code should be a focus of future development."

258
259 *Figures:*

260
261 - Fig. 1: *Higher resolution on detailed photos needed. This may have just been the pdf conversion*
262 *that shouldn't be an issue if high-resolution pictures provided for final publication. Otherwise, the*
263 *thorough photographic documentation is a nice inclusion.*

264
265 We will work with the editor to ensure high quality images.

266
267 - Fig. 1b "internals" photo: *black label too hard to read on dark background. Try white or yellow*
268 *and move to the right.*

269
270 We moved "internals" to the center of the insert, and changed the font color to white.

271
272 - Fig. 2: *all text too small (axes labels, tick label). Also x-axes labels on two plots on left are hiding*
273 *behind data*

274
275 We restructured Fig. 2 accordingly, incorporating requests from Reviewer 2 as well.

276
277
278
279
280
281
282
283
284
285
286
287

288
289
290
291

292
293
294
295
296

297
298
299
300

301
302
303
304
305

306
307
308
309
310
311

312
313

314
315

- Fig. 4. Units for velocity missing. Also, the colorbar and labels are too small.

Insert (e) represents a vector field for the velocity, so units are not needed. We stated this in the caption for clarification. The legend size cannot be changed as it comes out of OpenFOAM this way.

References

Huang, Y., Coggon, M. M., Zhao, R., Lignell, H., Bauer, M. U., Flagan, R. C. and Seinfeld, J. H.: The Caltech Photooxidation Flow Tube Reactor – I: Design and Fluid Dynamics, *Atmospheric Meas. Tech. Discuss.*, 1–36, doi:10.5194/amt-2016-282, 2016.

Lambe, A., Massoli, P., Zhang, X., Canagaratna, M., Nowak, J., Daube, C., Yan, C., Nie, W., Onasch, T., Jayne, J., Kolb, C., Davidovits, P., Worsnop, D. and Brune, W.: Controlled nitric oxide production via O(1D) + N₂O reactions for use in oxidation flow reactor studies, *Atmospheric Meas. Tech.*, 10(6), 2283–2298, doi:10.5194/amt-10-2283-2017, 2017.

Lambe, A. T., Ahern, A. T., Williams, L. R., Slowik, J. G., Wong, J. P. S., Abbatt, J. P. D., Brune, W. H., Ng, N. L., Wright, J. P., Croasdale, D. R., Worsnop, D. R., Davidovits, P. and Onasch, T. B.: Characterization of aerosol photooxidation flow reactors: heterogeneous oxidation, secondary organic aerosol formation and cloud condensation nuclei activity measurements, *Atmospheric Meas. Tech.*, 4(3), 445–461, doi:10.5194/amt-4-445-2011, 2011.

Li, R., Palm, B. B., Ortega, A. M., Hlywiak, J., Hu, W., Peng, Z., Day, D. A., Knote, C., Brune, W. H., de Gouw, J. A. and Jimenez, J. L.: Modeling the Radical Chemistry in an Oxidation Flow Reactor: Radical Formation and Recycling, Sensitivities, and the OH Exposure Estimation Equation, *J. Phys. Chem. A*, 119(19), 4418–4432, doi:10.1021/jp509534k, 2015.

Palm, B. B., Campuzano-Jost, P., Day, D. A., Ortega, A. M., Fry, J. L., Brown, S. S., Zarzana, K. J., Dube, W., Wagner, N. L., Draper, D. C., Kaser, L., Jud, W., Karl, T., Hansel, A., Gutiérrez-Montes, C. and Jimenez, J. L.: Secondary organic aerosol formation from in situ OH, O₃, and NO₃ oxidation of ambient forest air in an oxidation flow reactor, *Atmospheric Chem. Phys.*, 17(8), 5331–5354, doi:10.5194/acp-17-5331-2017, 2017.

Palm, B. B., de Sá, S. S., Day, D. A., Campuzano-Jost, P., Hu, W., Seco, R., Sjostedt, S. J., Park, J.-H., Guenther, A. B., Kim, S., Brito, J., Wurm, F., Artaxo, P., Thalman, R., Wang, J., Yee, L. D., Wernis, R., Isaacman-VanWertz, G., Goldstein, A. H., Liu, Y., Springston, S. R., Souza, R., Newburn, M. K., Alexander, M. L., Martin, S. T. and Jimenez, J. L.: Secondary organic aerosol formation from ambient air in an oxidation flow reactor in central Amazonia, *Atmospheric Chem. Phys.*, 18(1), 467–493, doi:10.5194/acp-18-467-2018, 2018.

Peng, Z. and Jimenez, J. L.: Modeling of the chemistry in oxidation flow reactors with high initial NO, *Atmospheric Chem. Phys.*, 17(19), 11991–12010, doi:10.5194/acp-17-11991-2017, 2017.

Peng, Z., Day, D. A., Stark, H., Li, R., Lee-Taylor, J., Palm, B. B., Brune, W. H. and Jimenez, J. L.: HO_x radical chemistry in oxidation flow reactors with low-pressure mercury lamps

316 systematically examined by modeling, *Atmospheric Meas. Tech.*, 8(11), 4863–4890,
317 doi:10.5194/amt-8-4863-2015, 2015.

318 Peng, Z., Day, D. A., Ortega, A. M., Palm, B. B., Hu, W., Stark, H., Li, R., Tsigaridis, K., Brune,
319 W. H. and Jimenez, J. L.: Non-OH chemistry in oxidation flow reactors for the study of
320 atmospheric chemistry systematically examined by modeling, *Atmospheric Chem. Phys.*, 16(7),
321 4283–4305, doi:10.5194/acp-16-4283-2016, 2016.

322 Peng, Z., Palm, B. B., Day, D. A., Talukdar, R. K., Hu, W., Lambe, A. T., Brune, W. H. and
323 Jimenez, J. L.: Model Evaluation of New Techniques for Maintaining High-NO Conditions in
324 Oxidation Flow Reactors for the Study of OH-Initiated Atmospheric Chemistry, *ACS Earth Space*
325 *Chem.*, doi:10.1021/acsearthspacechem.7b00070, 2017.

326

327 **RESPONSE TO REVIEWER 2: Manuscript ID: amt-2017-352**

328

329 *Mitroo et al. introduce a method to deconvolve the measured residence time distribution (RTD)*
330 *from sampling tubes to get the real RTD inside the Washington University Potential Aerosol Mass*
331 *(WU-PAM) reactor, which is also validated by computational fluid dynamic (CFD) simulation.*
332 *The idea of this paper can help improve the understanding of RTD for the oxidative flow reactor*
333 *(OFR) user community. This paper is well-written and fits the scope of AMT. I suggest for*
334 *publication after considering the following aspects:*

335

336 We thank the referee for their time in reading and reviewing this manuscript.

337

338 **[In reference to: General Comments]**

339

340 *1. I agree with Review #2's comments about the expansion of Section "5 Potential implication".*
341 *My concern is that how your method can be applied to simulation rather than just used to explain*
342 *RTD. In other words, how does the incorporation of CSTR tank-in-series (TIS) model framework*
343 *behave when compared with the PFR framework? For example, most of your inversion results*
344 *indicate that the number of TIS, N , is a little bit larger than 1. Does that mean it is CSTR rather*
345 *than PFR that can better represent OFR? So to simulate what happens in OFR, we should use*
346 *CSTR model instead of PFR? Then the question is to what extent the difference will be introduced*
347 *to the simulated results by shifting from PFR to CSTR. I think the authors should clarify these*
348 *points in this section.*

349

350 The referee is correct that given the number of TIS is a little bit larger than 1, the reactor
351 is considered to behave more like a CSTR than as a PFR. We address comments for both
352 referees in the revised manuscript (lines 406-434):

353

354 “Initial PAM modeling work assumed plug flow behavior in OFRs (Li et al., 2015). Li et
355 al. stated that correcting for the non-ideal E-Curve in their OFR would account for ~10%
356 error in their oxidant exposure results, which is less than the overall model uncertainty.
357 However, recent work incorporates the effect of non-ideal RTDs on model outputs (Palm
358 et al., 2017, 2018, Peng et al., 2015, 2016; Peng and Jimenez, 2017). Peng et al. (2015)
359 show that for three OFR operational modes (that is, modes of different oxidant formation

360 mechanisms denoted by ‘OFR185’, ‘OFR254-70’, and ‘OFR254-7’), a comparison
361 between model output for ideal plug flow vs. non-ideal RTDs (using the RTD
362 experimentally obtained by Lambe et al., 2011a) for OH exposure (OH_{exp}) generally agree
363 within a factor of 2 for low OH_{exp} ; the model disagreement exacerbates at high OH_{exp}
364 beyond a factor of ~ 4 . Peng and Jimenez then extend OFR operational modes to include
365 N-containing chemistry (in modes referred to therein as ‘OFR185-iNO’, ‘OFR185-7-iNO’,
366 and ‘OFR185-70-iNO’) where at moderate-to-high OH_{exp} , the deviations exacerbate
367 significantly, although the authors argue those conditions represent unrealistic chemical
368 pathways. It is worthwhile noting that the chemistry modeled by Peng and Jimenez may
369 find a workaround by utilizing N_2O as NO precursor (Lambe et al., 2017) rather than NO
370 itself, potentially minimizing RTD-related errors. Palm et al. (2018) report data from OFR
371 field deployment where the same comparison (ideal plug flow vs. the RTD experimentally
372 obtained by Lambe et al., 2011a) suggests RTD-related errors overpredict (for CO) or
373 underpredict (for toluene and monoterpenes) photochemical age (that is, the ratio of OH_{exp}
374 to tropospheric average OH number concentrations) in the reactor, generally within a factor
375 of 3 of model error. Considering this work employs the compartmental model RTD
376 described by Lambe et al. (2011a), which for reasons mentioned in the previous section
377 may not be the true PAM RTD, and given that non-ideality in RTDs affects certain OFRs
378 more than others, implementing the method presented here to obtain a more representative
379 reactor RTD can either help constrain error uncertainty in the models, or possibly extend
380 the OH_{exp} range in which OFRs can be operated, a reportedly nontrivial task (Palm et al.,
381 2018). Considering our results indicate that OFRs like the WU-PAM exhibit an RTD
382 closely matching that of an ideal CSTR, which is more well-mixed than the Lambe et al.
383 RTD, the sensitivity analysis conducted so far could represent a lower bound for error
384 analysis because the Lambe et al. RTD is closer to a PFR-like RTD than a CSTR-like
385 RTD.”

386
387 *2. TIS model can have different forms. The authors assume the same residence time for each CSTR-*
388 *tank and find the tank number. One can also take the form with a fixed CSTR (or PFR or mixed*
389 *CSTR/PFR) number but to find each residence time, which looks more reasonable given the CFD*
390 *simulation. Can the authors discuss this a little bit more? For example: How does the number of*
391 *TIS, N , depend on the flow rate, or in other words the average residence time? Since the flow rate*
392 *changes the fluid field, the mixing style could be different at different flow rates (e.g. Fig.3a-c).*
393 *But I cannot see any trend. Can the author give some explanation for that?.*

394
395 The classic TIS model assumes constant mean residence time across the N tanks, which is
396 $\bar{t}_i = \bar{t}/N$. In this work it is treated as a two-parameter model in which both N and \bar{t} are
397 scanned to find the optimum value pair that results in the best fit with experimental data. It
398 is found that the calculated mean residence time \bar{t} is similar to the space-time τ as
399 expected. Theoretically we can use any well-defined reactor model in place of TIS, such
400 as the axial dispersion model (ADM) (employed by Lambe et al., 2011a in tandem with
401 compartmental modeling) which measures the non-ideality from PFR. Mixed CSTR/PFR
402 is also possible, provided the mathematical derivation is properly carried out. Developing
403 such a new model is out of the scope of the current manuscript, but can be recommended
404 as future work in this field. Whether the reactor model selected is valid to represent the real
405 reactor is subject to validation with experimental measurements, as performed in Figure 3.

406 In this work we find the TIS model is satisfactory for the PAM reactor according to the
407 close agreement between model prediction and experimental data, stating the caveat that
408 the TIS model is *not* phenomenological. The reviewer raised the question about unclear
409 trend between N and space-time in Figure 3(a-c), which is interesting to the authors too.
410 Our guess is that under these conditions the reactor behaves so similarly to a single CSTR
411 that the subtle differences are buried in the experimental uncertainties. Perhaps the trend
412 would become more clear as the space-time is further raised, and we predict the trend to be
413 N increasing with space-time. The reason is that the larger the space-time, the slower the
414 flow, thus the weaker the turbulence and back-mixing, which means the further away the
415 reactor is from a single CSTR. This reasoning is backed by Figure 3f, where N is more
416 than doubled at a much higher space-time (although it is also a different configuration).

417
418 3. Equations in Appendix B should be carefully checked. For example, in Eq. (B3) it
419 should be $E_{i|N-i}$ instead of $E_{i|N-1}$. In addition, try to avoid “ N ”, since the number of
420 TIS is also “ N ”, which may cause confusion. In Eq. (B8), \mathbf{A} is a matrix, which should
421 be listed as A_{ij} not just $A_{n,i}$. One more, as a vector, \mathbf{B} should be listed as B_i , with
422 $i = 1, 2, \dots, N - 1$ and $i = N$. About time step Δt , see following comments for Figure 3.

423
424 We thank the referee for pointing out the inconsistent notations in the equations. The
425 misuse of indices can make the equations confusing and even wrong. We rewrote all of the
426 equations in Appendix B with carefully checked syntax. We hope they bring much more
427 clarity now. Please see revised manuscript lines 608-672.

428
429 **[In reference to: Specific Comments]**

430
431 1. Line 182: “create allow”, delete either one.

432
433 Similar to Reviewer 1, we thank the referee for pointing this out, and have deleted “allow”.

434
435 2. Line 218: “ F -curve”, define it here or mention it later

436
437 We restructured the sentences (L226-227 of the revised manuscript):

438
439 “After the simulation, the exit concentration is mixing-cup averaged to output a
440 representative of a cumulative RTD (explained in the next section).”

441
442 3. It is unnecessary to list both dimensional and non-dimensional equations at the same time, e.g.
443 EQ. 1-4 and 8-9, since the non-dimensional form has been introduced in detail in Appendix A

444
445 We respect the referee’s point of view, however we choose to represent both dimensional
446 and dimensionless equations in the main text for the audience.

447
448 4. Figure 2: Please use higher resolution figures and rearrange the figure locations (too compact,
449 and x -labels are hidden)

450
451 We restructured Fig. 2 accordingly, incorporating requests from Reviewer 1 as well.

453 5. Figure 3: Why time resolution is different in Panel e? Does Δt in Appendix B correspond to the
454 time interval in Figures 3a-f?

455
456 We had instrument problems that day, and could not take datapoints as frequently as for all
457 other panels. We have noted it in the figure caption. This doesn't affect the output of our
458 algorithm based on longer Δt .

459
460 "Lower frequency data for panel e) was due to instrument repair, and temporarily set on
461 longer averages."

462
463 6. Figure 5: Please use an intuitive y-label instead of "F". Also please specify "N" value in the
464 caption

465
466 We relabeled the y-axis with "Normalized Concentration" for easier interpretation The "N"
467 for the N-CSTR acronym the referee is referring to in the legend is another acronym for
468 the TIS model. We clarify this in the caption, and introduced this acronym along 'TIS' in
469 Section 3.2 (lines 313-317):

470
471 "We chose to apply the tank-in-series (TIS) model (MacMullin and Weber Jr., 1935), also
472 referred to as N-CSTR model, to the convolution integral since it is a one parameter model
473 that, although not specific to flowtube, tubular, laminar, or plug-flow reactors, gives an
474 idea of where the reactor lies on the spectrum of mixed flow vs. plugged flow based on the
475 value of a parameter, N "

476 477 **References**

478
479 Lambe, A., Massoli, P., Zhang, X., Canagaratna, M., Nowak, J., Daube, C., Yan, C., Nie, W.,
480 Onasch, T., Jayne, J., Kolb, C., Davidovits, P., Worsnop, D. and Brune, W.: Controlled nitric oxide
481 production via O(1D) + N₂O reactions for use in oxidation flow reactor studies, Atmospheric
482 Meas. Tech., 10(6), 2283–2298, doi:10.5194/amt-10-2283-2017, 2017.

483 Li, R., Palm, B. B., Ortega, A. M., Hlywiak, J., Hu, W., Peng, Z., Day, D. A., Knote, C., Brune,
484 W. H., de Gouw, J. A. and Jimenez, J. L.: Modeling the Radical Chemistry in an Oxidation Flow
485 Reactor: Radical Formation and Recycling, Sensitivities, and the OH Exposure Estimation
486 Equation, J. Phys. Chem. A, 119(19), 4418–4432, doi:10.1021/jp509534k, 2015.

487 Palm, B. B., Campuzano-Jost, P., Day, D. A., Ortega, A. M., Fry, J. L., Brown, S. S., Zarzana, K.
488 J., Dube, W., Wagner, N. L., Draper, D. C., Kaser, L., Jud, W., Karl, T., Hansel, A., Gutiérrez-
489 Montes, C. and Jimenez, J. L.: Secondary organic aerosol formation from in situ OH, O₃, and NO₃
490 oxidation of ambient forest air in an oxidation flow reactor, Atmospheric Chem. Phys., 17(8),
491 5331–5354, doi:10.5194/acp-17-5331-2017, 2017.

492 Palm, B. B., de Sá, S. S., Day, D. A., Campuzano-Jost, P., Hu, W., Seco, R., Sjostedt, S. J., Park,
493 J.-H., Guenther, A. B., Kim, S., Brito, J., Wurm, F., Artaxo, P., Thalman, R., Wang, J., Yee, L. D.,
494 Wernis, R., Isaacman-VanWertz, G., Goldstein, A. H., Liu, Y., Springston, S. R., Souza, R.,
495 Newburn, M. K., Alexander, M. L., Martin, S. T. and Jimenez, J. L.: Secondary organic aerosol

496 formation from ambient air in an oxidation flow reactor in central Amazonia, *Atmospheric Chem.*
497 *Phys.*, 18(1), 467–493, doi:10.5194/acp-18-467-2018, 2018.

498 Peng, Z. and Jimenez, J. L.: Modeling of the chemistry in oxidation flow reactors with high initial
499 NO, *Atmospheric Chem. Phys.*, 17(19), 11991–12010, doi:10.5194/acp-17-11991-2017, 2017.

500 Peng, Z., Day, D. A., Stark, H., Li, R., Lee-Taylor, J., Palm, B. B., Brune, W. H. and Jimenez, J.
501 L.: HO_x radical chemistry in oxidation flow reactors with low-pressure mercury lamps
502 systematically examined by modeling, *Atmospheric Meas. Tech.*, 8(11), 4863–4890,
503 doi:10.5194/amt-8-4863-2015, 2015.

504 Peng, Z., Day, D. A., Ortega, A. M., Palm, B. B., Hu, W., Stark, H., Li, R., Tsigaridis, K., Brune,
505 W. H. and Jimenez, J. L.: Non-OH chemistry in oxidation flow reactors for the study of
506 atmospheric chemistry systematically examined by modeling, *Atmospheric Chem. Phys.*, 16(7),
507 4283–4305, doi:10.5194/acp-16-4283-2016, 2016.

508 Peng, Z., Palm, B. B., Day, D. A., Talukdar, R. K., Hu, W., Lambe, A. T., Brune, W. H. and
509 Jimenez, J. L.: Model Evaluation of New Techniques for Maintaining High-NO Conditions in
510 Oxidation Flow Reactors for the Study of OH-Initiated Atmospheric Chemistry, *ACS Earth Space*
511 *Chem.*, doi:10.1021/acsearthspacechem.7b00070, 2017.

512

514

515 **Assessing the degree of plug flow in oxidation flow reactors (OFRs): a study on a Potential**
516 **Aerosol Mass (PAM) reactor**

517

518 Dhruv Mitroo^{1,a,*}, Yujian Sun^{1,*}, Daniel P. Combest², Purushottam Kumar³, and Brent J.
519 Williams¹

520

521 ¹Department of Energy, Environmental & Chemical Engineering, Washington University in St.
522 Louis, St. Louis, MO, USA

523 ²ENGYS, Ltd.

524 ³Discipline of Chemical Engineering, Indian Institute of Technology Gandhinagar, Palaj, Gujarat
525 382355, India

526

527 ^aNow at the Department of Atmospheric Sciences, Rosenstiel School of Marine and Atmospheric
528 Sciences, University of Miami, Miami, FL, USA

529

530 *equally contributing authors

531

532 Correspondence to: brentw@wustl.edu

533

534 Raymond R. Tucker I-CARES Career Development Associate Professor

535

536 Department of Energy, Environmental & Chemical Engineering
Washington University in St. Louis

537

538 **Abstract**

539

540 Oxidation flow reactors (OFRs) have been developed to achieve high degrees of oxidant exposures
541 over relatively short space times (defined as the ratio of reactor volume to the volumetric flowrate).

542 While, due to their increased use, attention has been paid to their ability to replicate realistic
543 tropospheric reactions by modeling the chemistry inside the reactor, there is a desire to customize

544 flow patterns. This work demonstrates the importance of decoupling tracer signal of the reactor
545 from that of the tubing when experimentally obtaining these flow patterns. We modeled the

546 residence time distributions (RTDs) inside the Washington University Potential Aerosol Mass
547 (WU-PAM) reactor, an OFR, for a simple set of configurations by applying the tank-in-series (TIS)

548 model, a one parameter model, to a deconvolution algorithm. The value of the parameter, N , is
549 close to unity for every case except one having the highest space time. Combined, the results

550 suggest that volumetric flowrate affects mixing patterns more than use of our internals. We
551 selected results from the simplest case, at 78s space time with one inlet and one outlet, absent of

552 baffles and spargers, and compared the experimental F-Curve to that of a computational fluid
553 dynamics (CFD) simulation. The F-Curves, which represents the cumulative time spent in the

554 reactor by flowing material, match reasonably well. We value that the use of a small aspect ratio
555 reactor such as the WU-PAM reduces wall interactions, and suggest applying the methodology of

556 tracer testing described in this work to investigate RTDs in OFRs and modify inlets, outlets, and
557 use of internals prior to applications (e.g., field deployment vs. laboratory study).

558

559 **1 Introduction**

560
561 Tubular reactors were first introduced to the field of atmospheric science by means of small flow
562 cell reactors developed to study the kinetics of stratospheric reactions (Brune et al., 1983; Howard,
563 1979; Keyser, 1980; Lamb et al., 1983). Accurate kinetic measurements were possible due to the
564 high pipe aspect ratios, which encouraged a high degree of plug flow behavior (Keyser, 1984).
565 The design of these miniature tubular reactors, with volumes on the order of a few cm³, was
566 different from that of significantly larger, batch-type or semi-continuous type well mixed reactors,
567 with volumes on the order of several m³, built to understand aerosol formation in the troposphere
568 (Crump et al., 1982; Crump and Seinfeld, 1980; Leone et al., 1985). To study aerosol formation
569 and growth chemistry, the dynamics of atmospheric circulation and transport needed to be
570 excluded. It was therefore convenient to mimic the troposphere by treating it as an enormous, well
571 mixed reactor, which led to the development of larger well mixed reactors. The discovery of
572 secondary processes preceding aerosol formation led to significant emphasis on the study of
573 secondary organic aerosol (SOA) formation (Haagen-Smit, 1952, 1963, 1970; Went, 1960). The
574 approach of using large, well mixed batch-style environmental chambers eventually helped
575 elucidate chemical mechanisms for model compounds (Claeys, 2004; Kamens et al., 1982; Kroll
576 et al., 2006; Nozière et al., 1999; Paulson et al., 1990; Pereira et al., 2015; Volkamer et al., 2001),
577 and, with improved instrumentation (Canagaratna et al., 2007; Crouse et al., 2006; de Gouw and
578 Warneke, 2007; Hansel et al., 1995; Jayne et al., 2000; Williams et al., 2006; Zhao et al., 2013),
579 the community gained a better understanding of SOA formation. Unfortunately, low levels of
580 conversion and high wall losses seen in these large reactors did not allow simulated exposures that
581 exceeded a day at most, which is just a short glimpse into the average two week lifespan of an
582 atmospheric aerosol (Seinfeld and Pandis, 2006). Due to such limitations, oxidation flow reactors

583 (OFRs) with short spacetimes (ratio of reactor volume to the volumetric flowrate) are being
584 developed (Cazorla and Brune, 2010; Ezell et al., 2010; George et al., 2007; Huang et al., 2016;
585 Kang et al., 2007).

586
587 OFRs can be viewed as tubular reactors due to their pipe aspect. They have been widely used for
588 over a decade to study heterogeneous reactions on organic aerosol surfaces involving gas-phase
589 oxidants such as hydroxyl radicals and ozone (George et al., 2007; George and Abbatt, 2010;
590 Katrib et al., 2005; Kessler et al., 2010, 2012; Knopf et al., 2005; Kroll et al., 2012; Smith et al.,
591 2009). These reactors are able to generate very high concentrations of hydroxyl (OH) radicals, tens
592 to thousands times higher than typical tropospheric levels, which accelerates the rate of gas-phase
593 oxidation reactions. Within spacetimes of a few minutes, it is possible to achieve integrated oxidant
594 exposures equivalent to multiple days or weeks of atmospheric oxidation. It is important to
595 distinguish OFRs from modern day conventional flow tube reactors, which stem from designs of
596 old flow tube reactors (e.g., Keyser 1984) but employed in the study of gas uptake kinetics on
597 aerosol surfaces rather than homogeneous gas-phase reactions, as described in the previous
598 paragraph. Beyond the original application of heterogeneous oxidation studies, Kang et al.
599 introduced the potential aerosol mass (PAM) OFR which, alongside newer OFR designs, was
600 intended specifically for studies of SOA physicochemical properties (Kang et al., 2007, 2011;
601 Keller and Burtscher, 2012; Lambe et al., 2011b, 2012, 2013; Massoli et al., 2010; Ortega et al.,
602 2013; Slowik et al., 2012). This application therefore altered the study of SOA formation,
603 previously dominated by the traditional large, well mixed reactors (Kroll and Seinfeld, 2008;
604 Rudich et al., 2007; Turpin et al., 2000), by allowing to generate laboratory data beyond first
605 simulated day of exposure. Because the mechanism of exposure between traditional chambers

606 OFRs was different, validating the OFR concept began by replicating data obtained from
607 traditional chambers (Chhabra et al., 2015; Lambe et al., 2015; Liu et al., 2015), and to assess
608 whether the chemistry was realistic (Li et al., 2015; McNeill et al., 2008; Peng et al., 2015;
609 Renbaum and Smith, 2011). Consequently, much modeling work has focused on pure chemical
610 reactions and comparison of SOA yields between the two (Bruns et al., 2015; Lambe et al., 2015;
611 Li et al., 2015; Ortega et al., 2016; Peng et al., 2015)(~~Bruns et al., 2015; Lambe et al., 2015; Li et~~
612 ~~al., 2015; Ortega et al., 2015; Peng et al., 2015~~). However, essentially no little modeling work has
613 been done on understanding hydrodynamics or flow fields inside OFRs so that the flow patterns
614 can be improved. In a study from Li et al., it appears that residence time distributions (RTDs) that
615 deviate significantly from plug flow in the PAM result only in a ~10% error of reported values
616 such as OH exposure (Li et al., 2015), which is conducive to OFRs being viewed as tubular
617 reactors. Following an experimentally determined RTD (Lambe et al., 2011) in a PAM OFR, Peng
618 et al. extend the model developed by Li et al., to include this non-ideal RTD, suggesting model
619 disagreement at high exposures. Ortega et al. employ FLUENT to show that removal of the inlet
620 plate (resulting in a less pronounced aperture to the reactor) significantly decreases recirculation
621 regions; and Palm et al. then extend the simulation to show that the FLUENT-derived RTD (Palm
622 et al., 2017) has a narrower distribution than the experimentally-derived RTD by Lambe et al.
623 Finally, Peng and Jimenez lay an initial framework for the possibility of OFRs investigating NO
624 chemistry (Peng and Jimenez, 2017), where initial sensitivity analysis on RTDs suggest
625 considerable model disagreement at high exposures. The fundamental caveat in this recent work
626 is the reliance on an accurately determined experimental RTD, that provides the basis for error
627 analysis. It is unknown if the error may trend with external OH reactivity (OHR_{ext}) and become

628 ~~more significant for slow reacting compounds, although efforts by the Jimenez Group at the~~
629 ~~University of Colorado at Boulder are underway.~~

630
631 In both single and multiphase reactors, contact patterns and the degree of mixing determine reactor
632 performance, e.g., selectivity and yield (Bourne, 2003; Deckwer, 1976; Levenspiel, 1999). This
633 implies that upon desired contacting, chemical pathways that would be otherwise suppressed can
634 become more competitive. For example, if during a mixed OH / ozonolysis heterogeneous
635 reaction, a fresh biomass burning aerosol is introduced in the centerline port of an OFR and ozone
636 is introduced along a side port, most of the aerosol may travel ballistically through the chamber
637 having limited contact with ozone or OH, and chemical reaction is less competitive with photolysis
638 / photobleaching reactions of the aerosol. RTDs describe the probability of a fluid element's age
639 inside the reactor: one can think of those as the probability distribution function (PDF) of a fluid
640 element in the reactor (Fogler, 2006; Levenspiel, 1999). Tools are available to diagnose or predict
641 flow behavior. These tools fall in two categories: tracer tests (diagnostics) and computational fluid
642 dynamics (CFD) simulations (predictions).

643
644 We present a technique to assess the degree of plug flow in an OFR, that can be in principle
645 extended to any vessel. The rigor of the technique is tested by varying use of internals and flowrate
646 and observing the resulting RTD curves in the Washington University PAM (WU-PAM) reactor.
647 We begin by introducing an experimental method for obtaining the reactor RTD, which can be
648 applied to any other OFR, via inert tracer injections. From raw data, we explain how to obtain
649 PDFs. We chose to run CFD on the simplest design (a base case configuration) of the WU-PAM
650 reactor to gain hydrodynamics information. Finally, we compare results from tracer tests and CFD

651 for the base case. ~~We compare this approach to that of previous studies by Lambe et al. (2011a),~~
652 ~~Huang et al. (2016), and Simonen et al. (2016), which to the best of our knowledge are the only~~
653 ~~other studies to date that report experimentally-derived RTDs in OFRs.~~~~We compare this approach~~
654 ~~to that of previous studies by Lambe et al. (Lambe et al., 2011a), Huang et al. (Huang et al., 2016),~~
655 ~~and Simonen et al. (Simonen et al., 2016), to the best of our knowledge, the only other studies on~~
656 ~~RTDs in OFRs.~~ We do not provide predictive configurations for the PAM reactor because there
657 are many avenues different groups can take depending on their focus, and this study is central to
658 the current design.

659
660 **2 Methods**

661
662 The WU-PAM reactor is an iridite-treated aluminum cylinder, 18 inches in length and 8 inches in
663 inner diameter, giving it a total volume of 13 L. It has two 12 inch mercury lamps with peak
664 wavelengths at 185 nm and 254 nm (BHK Inc. Analamp Model No. 82-9304-03) housed in Teflon
665 sheaths, directly opposite each other, along the axial direction. Annular flow of N₂ (Airgas)
666 through the sheaths prevents direct contact with the lamps and purges any outgas products when
667 the lamps are turned on. The mercury lamps are left in place with their housing to mimic simple
668 OFR internals; they have not been turned on during this study. Details of their mode of operations
669 for oxidant formation can be found elsewhere (Li et al., 2015; Peng et al., 2015, 2016). OFRs like
670 the WU-PAM have removable internals, face plates, and peripheral inlets and outlets that allow a
671 wide variety of configurations. For example, Ortega et al. removed the inlet plate of their PAM
672 reactor during a deployment in the Fire Lab at Missoula Experiment (FLAME-3) while keeping
673 the inlet baffle to reduce particle loss, and in doing so observed a reduction in jetting of centerline

674 flow (Ortega et al., 2013). In a different study, Lambe et al. ran experiments keeping the inlet plate
675 on the PAM coupled with a sparger (a cap with large holes in the side in fixed onto the inlet, so
676 that the flow does not jet into the chamber), because laboratory experiments required a closed
677 system (Lambe et al., 2011a).

678
679 In this work, we chose four configurations: I (one inlet, one outlet, two lamp housings as internals),
680 II (one inlet, one outlet, two lamp housings with sparger and baffles as internals), III (multiple
681 inlets, multiple outlets, two lamp housings as internals), and IV (multiple inlets, one outlet, two
682 lamp housings with sparger and baffles as internals). Configuration I at 78s spacetime was subject
683 to a CFD simulation as a simple scenario where the simulation could capture hydrodynamics
684 accurately.

685

686 **2.1 Tracer studies**

687

688 The laboratory setup to determine RTDs experimentally is shown in Fig. 1. N₂ (Airgas) was the
689 carrier fluid and SO₂ (3 ppm; Air Liquide) was the inert tracer. Both flow rates were controlled by
690 mass flow controllers (MFCs) (Pneucleus Technologies, LLC). All experiments began by allowing
691 one hour to achieve a steady state of the carrier gas' flow profile inside the reactor, after which
692 SO₂ was introduced in a single step-up manner. A tracer flowrate of 100 cm³ min⁻¹ allowed good
693 detection in the measurement and minimized perturbation of the flow field. Analogously, the flow
694 of the carrier fluid was stepped down to maintain a constant desired total volumetric flowrate. SO₂
695 mixing ratios were determined by a Trace level-Enhanced SO₂ Analyzer (Thermo Scientific Model
696 43i, Thermo Scientific) via pulsed fluorescence, and the instrument was set to an averaging time

697 of 10s. This setting was the highest frequency over which the instrument could average the signal.
698 Obtaining high frequency data simplifies data analysis by avoiding the need for interpolation
699 techniques, as discussed in Sect. S1.

700

701 We expected that the tracer would experience an associated spacetime and RTD in places other
702 than the reactor, between the exit of the flow controller and the SO₂ detection chamber in the gas
703 analyzer. We therefore ran two experiments for every WU-PAM reactor configuration. The first
704 incorporated both the reactor and the inlet and outlet plumbing, and the second bypassed the
705 reactor. From these two signals we could extract the actual reactor RTD as described in Sect. 3.2.
706 Both experiments were operated by allowing the formation of fully developed flow before
707 injecting the tracer stepwise, as mentioned previously. Appendix A describes in detail how we
708 obtained a PDF and a cumulative distribution function (CDF) from raw data.

709

710 The WU-PAM reactor has peripheral inlets and outlets to optionally create ~~allow~~ a ring (annular)
711 flow around the centerline. Ideally, a uniformly distributed flow around the centerline helps
712 stabilize the flow, avoids recirculation, and reduces wall losses. To create ring flow, we formed a
713 three-eighth inch Teflon tube into a circle, and drilled six one-sixteenth inch diameter holes evenly
714 spaced along the side of the tube facing in the direction of flow. A similar Teflon tube circle was
715 created for the outflow. The ring flow setup required additional plumbing internals (Fig. 1b).
716 Tracer tests were accomplished for configuration I at three different spacetimes (of 52s, 78s, and
717 152s), for three different configurations (I, II, and III) at a 78s spacetime, and an arbitrary special
718 case for configuration IV at 411s spacetime (configuration and spacetime not commonly used).

719

720 2.2 Simulations

721

722 While tracer studies are a powerful diagnostic tool and result, if done correctly, in accurate RTDs,
723 they cannot capture the full hydrodynamics details, or the state of mixing in the reactor (i.e., the
724 exchange of mass between the fluid elements). Both hydrodynamics and mixing can significantly
725 influence the reactor performance (Fogler, 2006; Villermaux, 1986). For configuration I at 78s
726 spacetime, we ran a CFD simulation to visualize the hydrodynamics inside the WU-PAM. This
727 comparative analysis seeks to provide validation prior to using the CFD platform as a predictive
728 tool for mixing patterns in OFRs with more complex geometry or internals.

729

730 As a solver, we used OpenFOAM, an open source CFD toolbox available at www.openfoam.com
731 or www.openfoam.org. The reactor geometries were constructed on FreeCAD, an open source
732 computer aided design (CAD) software available at www.freecadweb.org, and Onshape, available
733 at www.onshape.com, prior to being exported into OpenFOAM. To discretize the volume elements
734 in the geometry, a mesh was created using the snappyHexMesh tool in OpenFOAM either directly
735 or in the HELYX-OS GUI. By generating mainly hexahedral meshes, this tool can mesh objects
736 of irregular shape. Then, additional layers of different geometry are added to the surface to improve
737 the mesh quality. A figure and details of the mesh can be found in Figure S1 and Table S1,
738 respectively. The hydrodynamics were calculated using simpleFoam, a steady-state solver for
739 single phase incompressible laminar or turbulent flow. We used ~~first~~-first-order schemes, and
740 specified the boundary conditions in each simulation case. The outlets had zero gradient for
741 velocity and fixed values for pressure, while the walls had fixed value for velocity and zero
742 gradient for pressure. After the flow field is obtained, a tracer experiment is simulated by

743 scalarTransportFoam for one of the simulations, which solves the transient convection-diffusion
744 transport equation of a passive scalar (dimensionless tracer concentration in this case). The initial
745 condition is zero concentration, and the boundary condition at the inlet is that the dimensionless
746 tracer concentration is equal to 1. After the simulation, the exit concentration is mixing-cup
747 averaged to output a representative of a cumulative RTD (explained in the next section).~~an F-~~
748 ~~Curve~~. We added a modification to the existing solver to account for turbulent diffusivity, which
749 had a non-negligible effect on mixing in the WU-PAM reactor, particularly at the entrance jet for
750 high flowrates. We found that the turbulent diffusivity was on the same order of magnitude as the
751 molecular diffusivity within the jet region near the inlet, suggesting turbulence in the jet was
752 significant. It is worthwhile to note that the inlet sparger and baffles (i.e., internals present in
753 configuration II and IV) left out of the simulation could significantly affect this outcome. However,
754 resolving the simulation mesh size to account for these internals significantly extended the
755 computational requirements, to the point that running these simulations was not possible on our
756 computer system and would require a computing cluster to perform. ~~however these simulations~~
757 ~~required significant computer time to resolve mesh sizing.~~

758

759 **3 Results**

760

761 **3.1 The RTD function, $E(t)$, and the cumulative RTD function, $F(t)$**

762

763 Tracer tests give us fast qualitative information about the reactor, but mathematical manipulation
764 (e.g., normalizing the data and scaling the axes) of the data provide quantitative information and
765 offers a basis for comparing reactor behaviors on a universal scale. The main mathematical

766 descriptors of a fluid element residing in a chamber are its PDF and its CDF. For a chemical
767 reactor, the PDF is more commonly referred to as the RTD function, $E(t)$, in the dimensional
768 domain, or $E(\theta)$ in the dimensionless domain (referred to as E-Curves). Similarly, the CDF is
769 called the cumulative RTD function, $F(t)$, in the dimensional domain, or $F(\theta)$ in the
770 dimensionless domain (referred to as F-Curves) (Danckwerts, 1953; MacMullin and Weber Jr.,
771 1935). The relations between E-Curves and F-Curves are derived for the reader in this Appendix
772 A, but are well established and available on the internet and in classical textbooks (Fogler, 2006;
773 Levenspiel, 1999, 2002).

774

775 Figure 2 gives an example of how mathematical processing of the data looks. The shape of the
776 curve does not change, but the axes do. Section S1 explains how we obtained a pulse response
777 equivalent of concentration data from stepwise addition of the tracer.

778

779 In the WU-PAM, advective flow should be the main form of transport (we do not consider
780 convective effects due to thermal gradients from lamp activity in this work). Modeling real reactors
781 can be challenging, but approximations are possible using ideal reactor concepts (Levenspiel,
782 2002). The two most common examples of ideal reactors are the plug flow reactor (PFR), where
783 the flow is perfectly plugged or piston-like, and the continuously stirred tank reactor (CSTR),
784 where the flow is perfectly mixed. Mathematically, their E-Curves are represented by Equations
785 1-4:

786

$$E_{PFR}(t) = \delta(t - \bar{t}) \quad (1)$$

$$E_{PFR}(\theta) = \delta(\theta - 1) \quad (2)$$

$$E_{CSTR}(t) = \frac{1}{\bar{t}} e^{-\frac{t}{\bar{t}}} \quad (3)$$

$$E_{CSTR}(\theta) = e^{-\theta}. \quad (4)$$

787

788 Examples of how RTDs look like based on compartmental modeling using both ideal reactors are
789 available in chemical engineering textbooks (Fogler, 2006; Levenspiel, 1999) and, although not
790 discussed here, a variety of phenomenological models can be applied to describe or compare
791 OFRs. It is then open to interpretation whether the combination of ideal reactors chosen for an E-
792 Curve (e.g., a PFR and CSTR in series, or two CSTRs in parallel) describes the hydrodynamics of
793 the reactor as well. The RTD of an OFR should be obtained experimentally, if possible, before
794 deciding what model to use to describe it. Development of a phenomenological model to describe
795 the WU-PAM RTD is beyond the scope of this study, whose aim is to develop a robust
796 methodology to assess degree of plug flow in any OFR, however is an avenue that should be
797 pursued in the future. Given our current setup at Washington University, the true reactor RTD is
798 impossible to measure accurately by a single tracer injection. The tubing length, pressure drop
799 inside the filter holder upstream of the SO₂ detector, and location of the SO₂ detector have not
800 been minimized, thus we expect that collectively they could perturb our measurements
801 significantly. We choose not to simply subtract the theoretical space time of the tubing, because
802 non-ideal tracer injection or detection are most likely not represented by a Dirac function of a
803 perfect impulse (or derived from a perfect stepwise injection, represented by the Heaviside
804 function). Therefore we need to deconvolute the RTD signal due to the reactor from the signal due
805 to additional plumbing.

806

807 **3.2 Tank-in-Series model for indirect deconvolution**

808

809 Levenspiel describes the convolution integral (Levenspiel, 1999) in his textbook “Chemical
810 Reaction Engineering”, which has been adapted to solve previous problems of decoupling RTD
811 signals (Hamed, 2012; Han, 2007; Mills and Duduković, 1988; Simonen et al., 2016; Sun, 2010).
812 This integral focuses on packets of the tracer that enter t' seconds before t , that is $(t - t')$, and
813 stay t' seconds in the reactor:

$$C_{out}(t) = \int_0^t C_{in}(t') \cdot E(t - t') dt', \quad (5)$$

814 or

$$C_{out}(t) = C_{in} * E \quad (6)$$

815 where E is the true E-Curve of the reactor, and C_{in} and C_{out} are the time-dependent concentration
816 profiles of the measured tracer at the injection port and outlet port respectively. This equation is
817 based on assumptions of mass conservation (i.e., no wall loss inside the reactor) and memory loss
818 (i.e., the fluid elements in fast-moving fluid in a region are not bound to behave as fast-moving in
819 another region). We separate two regions in our setup, and identify three E-Curves. These
820 correspond to curves for the reactor, the plumbing (including filters, instrument plumbing, and the
821 instrument detector chamber), and the two together. Respectively, we denote them as $E_0(t)$, $E_1(t)$,
822 and $E_2(t)$. We are able to accurately measure $E_2(t)$ and $E_1(t)$, but not $E_0(t)$. Thus, Eq. (6) now
823 takes the form

$$E_2(t) = E_0(t) * E_1(t), \quad (7)$$

824 and we need to solve for $E_0(t)$. Details of the deconvolution approach can be found in Appendix
825 B, however direct application of this technique failed to get the solution to converge. It is a robust
826 protocol to accurately determine a numerical RTD, and should be applied whenever a stable
827 solution is available.

828

829 What we propose is an indirect application, i.e., to guess $E_0(t)$ so that the convolution integral
830 yields a curve that matches that of $E_2(t)$. This requires a formidable number of guesses and
831 iterations and could be a lengthy process if done numerically. One workaround is to assume a form
832 of $E_0(t)$, ideally with one variable parameter, that can be tuned to give the $E_2(t)$ that best matches
833 the experimental $E_2(t)$ curve. The CSTR and PFR forms should not be considered since they are
834 ideal extremes of reactor behavior. We chose to apply the tank-in-series (TIS) model (MacMullin
835 and Weber Jr., 1935), also referred to as N-CSTR model, to the convolution integral since it is a
836 one parameter model that, although not specific to flowtube, tubular, laminar, or plug-flow
837 reactors, gives an idea of where the reactor lies on the spectrum of mixed flow vs. plugged flow
838 based on the value of a parameter, N . N refers to the fictitious number of equivalent CSTRs that,
839 in series, describe the E-Curve for the reactor. This function is

840

$$E(t) = \frac{t^{N-1}}{(N-1)! \left(\frac{\bar{t}}{N}\right)^N} e^{-\left(\frac{N}{\bar{t}}\right)t} \quad (8)$$

$$E(\theta) = \frac{N(N\theta)^{N-1}}{(N-1)!} e^{-N\theta}. \quad (9)$$

841

842 For a value of $N = 1$, the E-Curve becomes that of a perfect CSTR; for a value of $N = \text{infinity}$, it
843 becomes that of a perfect PFR, as shown in Fig. S2. Using this model, the convolution integral
844 takes the form

$$E_2^*(t) = \int_0^t E_1(t-t') \cdot \frac{t'^{N-1}}{(N-1)! \left(\frac{\bar{t}}{N}\right)^N} e^{-\left(\frac{N}{\bar{t}}\right)t'} dt', \quad (10)$$

845 where $E_1(t - t')$ is an array of accurate experimental data already obtained, and $E_2^*(t)$ is the
846 output guess. $E_2^*(t)$ is then matched to $E_2(t)$ by varying N in an iterative fashion. Using this form,
847 the algorithm in Appendix B is still valid. We used MATLAB to solve this for all cases. The results
848 are displayed in Fig. 3.

849

850 **4 Discussion**

851

852 The small aspect ratio of the WU-PAM limits wall interactions, preventing laminar flow
853 development due to absence of a boundary layer. This suggests the flow field would then depend
854 on inlet/outlet geometries or volumetric flowrate. Though, for a fixed spacetime of 78s, we
855 observed that different configurations had no significant effect on the RTD (Figs. 3b, d, e). Further,
856 for configuration I, different spacetimes also had no significant effect. The only case with a marked
857 change in the signal was for configuration IV at 411s spacetime (Fig. 3f). We attribute this
858 difference to the low volumetric flowrate, implying that advective transport begins to be less
859 dominant than turbulent or molecular diffusivity as mode of transport. Such a low spacetime, while
860 increasing the degree of plug flow, would result in a potentially significant loss of semivolatile or
861 low volatility gases. Additionally, other modes of transport such as convective effects (vertical
862 mixing for non-isothermal conditions) could become more apparent, as revealed by Huang et al.
863 for the Caltech photooxidation flow tube (CPOT) reactor. As mentioned earlier, a detailed
864 phenomenological modeling study of RTDs in the WU-PAM is beyond the scope of this study,
865 however at more conventional spacetimes, it would be helpful to visualize hydrodynamics to
866 assess what contacting patterns and state of mixing the reactor exhibits. We thus chose a simple
867 scenario as a base case for simulation: configuration I at 78s spacetime.

868

869 CFD reveals that the hydrodynamics inside the PAM are far from that of a well-mixed reactor (Fig.
870 4). This is insightful because the F-Curve of the simulation matches reasonably well with that of
871 the experiment (Fig. 5) and alone would imply CSTR-like mixing. This is the caveat associated
872 with interpreting RTDs, and further supports investigation in phenomenological modeling.
873 Snapshots of the simulation displayed in Fig. 4a-c show there is jetting (short-circuiting),
874 recirculation, and dead zones. Jetting leads to fluid elements that have a very short residence time
875 and cause high values of $E(t)$ at $t > 0s$. Recirculation leads to fluid elements spending more time
876 in the reactor, yielding middle values of $E(t)$ as elements exit at $t \sim \bar{t}$. Stagnation (dead zones) at
877 the inlet of the reactor cause fluid elements to remain entrained in the reactor for a long time before
878 exiting the reactor at $\sim 2-3$ times \bar{t} at low values of $E(t)$, leading to a long tail in the E-Curve. These
879 three effects together lead to an E-Curve that looks similar to that of a CSTR, but mixing in CSTRs
880 is dominated by recirculation; meaning that the local concentration of tracer at the exit is identical
881 to all other locations in the reactor (Zwietering, 1959). Therefore, while tracer tests give a general
882 idea about contacting patterns, CFD visualizes the hydrodynamics, and help model the reactor.
883 Plotting the WU-PAM OFR's E-Curves for this scenario on a semilog plot does not yield different
884 gradients, which would otherwise indicate different volumes for the compartmental modeling of
885 the jetting, recirculation, and dead volumes (Levenspiel, 2002). The limitation to that statement is
886 that the E-Curves in this work have been obtained by fitting a one-parameter model, consequences
887 of which should be the focus of future work in conjunction with phenomenological modeling.
888 Furthermore, our simulations are limited to isothermal conditions, therefore cannot predict
889 buoyancy effects that could explain spread in the RTD at low flowrates (or low Reynolds numbers)
890 (Fig. 3f), as observed by Huang et al. (2016).

891
892 Lambe et al. (2011a) modeled the Pennsylvania State University PAM (PSU-PAM) reactor using
893 a compartmental model consisting of two parallel tubular reactors that exhibit Taylor dispersion
894 (Taylor, 1953), suggesting that their reactor (whose geometry is identical to that of the WU-PAM
895 OFR) has two main volumes: an active reactor volume, and another volume with entrainment. The
896 model output matches their experimental data reasonably well, but, they did not decouple the
897 reactor's E-Curve from that of the setup, implying the match may include phenomena occurring
898 in other pipes of the setup. Lambe et al. describe RTDs for the two volumes using the axial
899 dispersion model (ADM) (Taylor, 1953, 1954a, 1954b), which is based on modeling plug or
900 laminar flow with axial dispersion of material. Generally, as also stated by Huang et al. (2016),
901 the ADM is valid for regions where the radial Péclet number (Pe_r) is less than ~ 4 times the aspect
902 ratio (length of reactor divided by its cross sectional area), or if Pe_r is greater than $\sqrt{48}$ (Aris, 1956;
903 Taylor, 1954b). Both the PSU-PAM OFR and the WU-PAM OFR meet these requirements under
904 typical flowrates (see SI, Sect. S4). If the reactor could be described by the ADM, CFD would
905 show that the entrance and exit effects would be separate from the main flow in the tube – which
906 is not the case for the simplified geometry of configuration I. We do not know how well they apply
907 to the other configurations. At no point inside the reactor does pipe flow fully develop, so the high
908 aspect ratio concept (Kang et al., 2007) does not allow a velocity profile to become established
909 with the current end caps used. Thus, although Pe_r appears acceptable, the inlet and outlet regions
910 should be re-engineered to allow formation of fully developed pipe flow in the main cylinder for
911 the ADM to be valid. While the E-Curve for configuration II is similar to that of configuration I at
912 78s spacetime, it would be helpful to run CFD on that configuration at different spacetimes to
913 observe if, and if so at what spacetime, the sparger and baffles efficiently suppress jetting.

914 Unfortunately, our CFD mesh could not be refined enough to capture the geometry of those without
915 sacrificing valuable computational time.

916
917 Instead, we chose to apply the use of an inlet cone (45° angle, 4.94'' length) and outlet peripherals
918 to simulate a more attenuated inlet and exit from sudden aperture. The results are displayed in Fig.
919 6. While the size of the jet appears to be broader compared to simulations in Fig. 5 (unaltered
920 PAM geometry), it is nonetheless present. Furthermore, recirculation in the form of backmixing is
921 evident towards the front, and stagnation close to the walls and corners persists. From the velocity
922 field (Fig. 6 center figure), a smaller cone angle that follows the contour of the light blue velocity
923 field could prevent backmixing.

924

925 **5 Potential implications**

926

927 Initial PAM modeling work assumed plug flow behavior in OFRs (Li et al., 2015). Li et al. stated
928 that correcting for the non-ideal E-Curve in their OFR would account for ~10% error in their
929 oxidant exposure results, which is less than the overall model uncertainty. However, recent work
930 incorporates the effect of non-ideal RTDs on model outputs (Palm et al., 2017, 2018, Peng et al.,
931 2015, 2016; Peng and Jimenez, 2017). Peng et al. (2015) show that for three OFR operational
932 modes (that is, modes of different oxidant formation mechanisms denoted by ‘OFR185’,
933 ‘OFR254-70’, and ‘OFR254-7’), a comparison between model output for ideal plug flow vs. non-
934 ideal RTDs (using the RTD experimentally obtained by Lambe et al., 2011a) for OH exposure
935 (OH_{exp}) generally agree within a factor of 2 for low OH_{exp}; the model disagreement exacerbates at
936 high OH_{exp} beyond a factor of ~4. Peng and Jimenez then extend OFR operational modes to include

937 N-containing chemistry (in modes referred to therein as ‘OFR185-iNO’, ‘OFR185-7-iNO’, and
938 ‘OFR185-70-iNO’) where at moderate-to-high OH_{exp} , the deviations exacerbate significantly,
939 although the authors argue those conditions represent unrealistic chemical pathways. It is
940 worthwhile noting that the chemistry modeled by Peng and Jimenez may find a workaround by
941 utilizing N_2O as NO precursor (Lambe et al., 2017) rather than NO itself, potentially minimizing
942 RTD-related errors. Palm et al. (2018) report data from OFR field deployment where the same
943 comparison (ideal plug flow vs. the RTD experimentally obtained by Lambe et al., 2011a) suggests
944 RTD-related errors overpredict (for CO) or underpredict (for toluene and monoterpenes)
945 photochemical age (that is, the ratio of OH_{exp} to tropospheric average OH number concentrations)
946 in the reactor, generally within a factor of 3 of model error. Considering this work employs the
947 compartmental model RTD described by Lambe et al. (2011a), which for reasons mentioned in the
948 previous section may not be the true PAM RTD, and given that non-ideality in RTDs affects certain
949 OFRs more than others, implementing the method presented here to obtain a more representative
950 reactor RTD can either help constrain error uncertainty in the models, or possibly extend the OH_{exp}
951 range in which OFRs can be operated, a reportedly nontrivial task (Palm et al., 2018). Considering
952 our results indicate that OFRs like the WU-PAM exhibit an RTD closely matching that of an ideal
953 CSTR, which is more well-mixed than the Lambe et al. RTD, the sensitivity analysis conducted
954 so far could represent a lower bound for error analysis because the Lambe et al. RTD is closer to
955 a PFR-like RTD than a CSTR-like RTD. Recent modeling work assumes plug flow behavior in
956 OFRs (Li et al., 2015; Peng et al., 2015, 2016). Li et al. state that correcting for the non-ideal E-
957 Curve in their OFR would account for ~10% error in their results, which is less than the overall
958 model uncertainty.

959

960 For compounds with low lifetimes to OH, contacting could influence the model results to a greater
961 extent (e.g., field deployment monoterpene decay reported by Palm et al., 2018). By taking a ratio
962 of characteristic reaction time to the characteristic transport time, one can define the Damköhler
963 number (Da_n). Considering spacetimes of 52-411s (as per this study), the value of Da_n can be
964 between 0.52 and 4.11 for a compound with lifetimes of ~100s. Since reaction timescales are on
965 the order of transport timescales, contact patterns may play an important role, as seen in Palm et
966 al. (2018). This could also be the case for heterogenous reactions, diffusion-limited reactions, or
967 semivolatile compound (SVOC) oxidation that exhibit slow gas-particle partitioning. Furthermore,
968 combining a phenomenological model to an associated RTD can impact kinetics (and yields)
969 further. The RTD generated by Lambe et al. (2011a) employed in Li et al. (2015) may lead to
970 greater than 10% error if the 2 PFRs in parallel model suggested by Lambe et al. (2011a) is not
971 applicable. In these scenarios, ensuring a high degree of plug flow can not only maximize
972 exposure, but minimize the distribution of aged compounds (e.g., first or second generation
973 compounds) that are due to different exit ages because of recirculation or stagnation. However,
974 this configuration may not suit a field deployment where trace compounds have short lifetimes to
975 OH and can be easily lost to reactor walls, in which case ensuring a high degree of mixing would
976 be beneficial.~~However, for compounds with low OHR_{ext} , contacting could influence the model~~
977 ~~results to a greater extent. By taking a ratio of characteristic reaction time (e.g., OHR_{ext}) to the~~
978 ~~characteristic transport time, one can define the Damköhler number (Da_n). Considering spacetimes~~
979 ~~of 52-411s (as per this study), the value of Da_n can be between 5200 and 41100 for a compound~~
980 ~~with $OHR_{ext} \sim 100s^{-1}$. Since reaction timescales are 10^4 times faster than transport timescales,~~
981 ~~contact patterns won't matter to a large degree. However, the value of Da_n can be between 5.2 and~~
982 ~~41.1 for a compound with $OHR_{ext} \sim 0.1s^{-1}$, in which case contacting patterns may play a more~~

983 significant role. This could be the case for heterogenous reactions, diffusion-limited reactions, or
984 semivolatile compound (SVOC) oxidation that exhibit slow gas-particle partitioning. Furthermore,
985 combining phenomenological model to an associated RTD can impact kinetics (and yields) further.
986 The RTD generated by Lambe et al. (2011) employed in Li et al. (2015) may lead to greater than
987 10% error if the 2-PFRs in parallel model suggested by Lambe et al. (2011) is not applicable. In
988 these scenarios, ensuring a high degree of plug flow can not only maximize exposure, but minimize
989 the distribution of aged compounds (e.g., first or second generation compounds) that are due to
990 different exit ages because of recirculation or stagnation. This configuration would suit a
991 laboratory experiment with slow kinetics, where concentrations can be made high enough to where
992 wall losses aren't an issue. However, this configuration may not suit a field deployment where
993 trace compounds have high OHR_{ext} and can be easily lost to reactor walls, in which case ensuring
994 a high degree of mixing would be beneficial.

995
996 We do recognize that OFR (or any environmental chemical reactor) users may have a preference
997 to rapidly obtain an RTD profile perhaps using an improvised setup with very short sample lines
998 and a fast time-response gas analyzer. However, the accuracy to which the profile is obtained
999 should be carefully examined. If the reactor is considerably large, or if it is an OFR to be deployed
1000 for low levels of exposure, then the influence of plumbing is minimal. If the reactor of choice is
1001 small, the oxidant exposure is high, or the reactor has more than one inlet/outlet or other peripheral
1002 components, it would be recommended to use the method described here to obtain the most
1003 representative RTD, since all sources of bias are removed.

1004 1005 **6 Conclusion**

1006

1007 The WU-PAM reactor's hydrodynamics are complex, and even though the E-Curve looks simple,
1008 applying a compartmental model (phenomenological modeling) to obtain an analytical E-Curve
1009 (rather than the empirically-based TIS E-Curve) can be challenging. Having too sudden an aperture
1010 at the entrance zone leads to dead volumes at the inlet corners. We cannot confirm if the sparger
1011 design helps reduce dead volume, but tracer tests suggest it doesn't appear to affect the degree of
1012 plug flow under standard operating spacetimes (52-156s). The reactor is described neither by back
1013 mixing, plug flow, nor by the ADM in any configuration. However, for configuration IV at 411s
1014 spacetime, a noticeable shift towards plug flow behavior is observed, perhaps due to a combined
1015 effect of internals and low inlet velocity. We note that the E-Curves we obtain are not as accurate
1016 as an E-Curve numerically obtained by direct deconvolution, since we are forcing a closed form
1017 solution on our data. We further note the need for phenomenological modeling.

1018

1019 Tapered ends on the inlet and the outlet would help to develop a steady flow profile at the inlet
1020 and avoid recirculation at the outlet, however the cone angle should be predetermined by CFD if
1021 possible. By improving simulations to include temperature gradients induced when the internal
1022 lamps are on, and refining the mesh to capture internals, the ADM should be revisited as a model
1023 to describe the PAM reactor. If the ADM satisfactorily describes the PAM reactor's RTD, kinetics
1024 should be easier to obtain, and diffusivity values using the Aris-Taylor relationship (Aris, 1956)
1025 can even be obtained. This could help assess whether processes are reaction limited or diffusion
1026 limited, arguing the reactor validity in experimental setups. At that point, the reactors would be
1027 regulated by only one parameter, their flowrate. This parameter would be adjusted to achieve
1028 desired spacetimes depending on OHR_{ext} . Finally, to obtain accurate experimental RTDs,

1029 achieving a functional direct deconvolution code should be a focus of future development. The
1030 implementation of this technique can be extended to drift tubes in mass spectrometers, as those are
1031 essentially flow tube reactors where ionization efficiency can be strongly influenced by mixing.

1032

1033 **Acknowledgements**

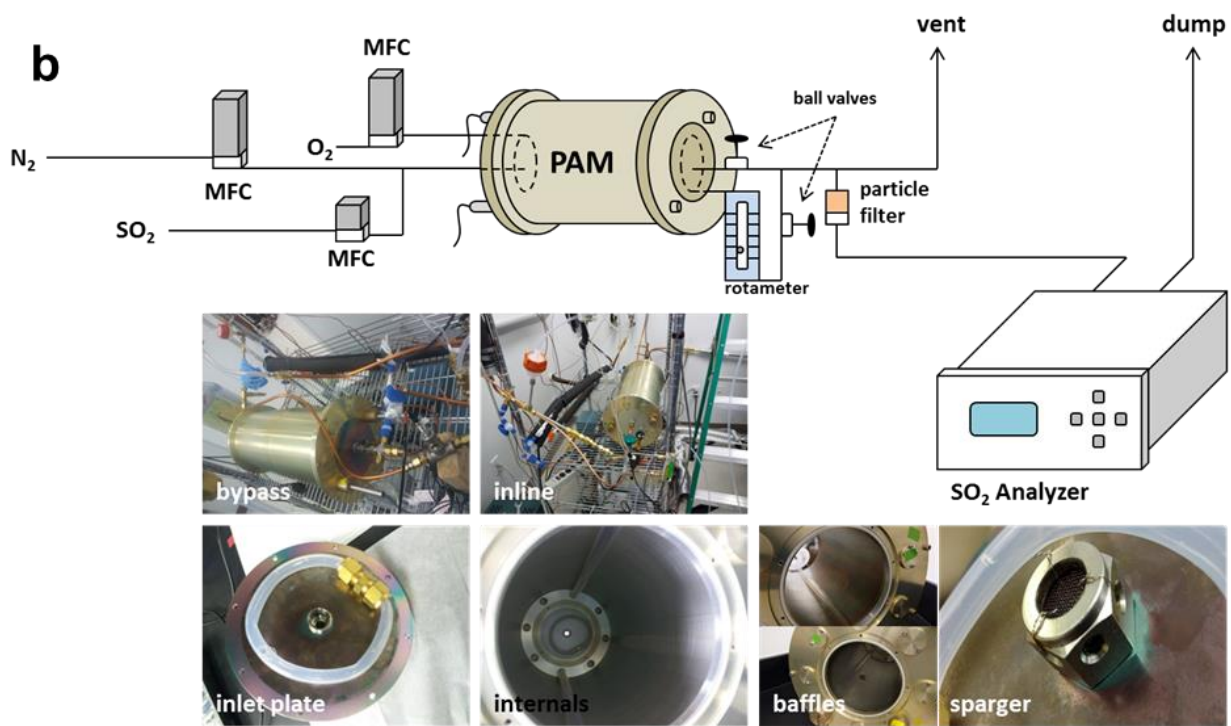
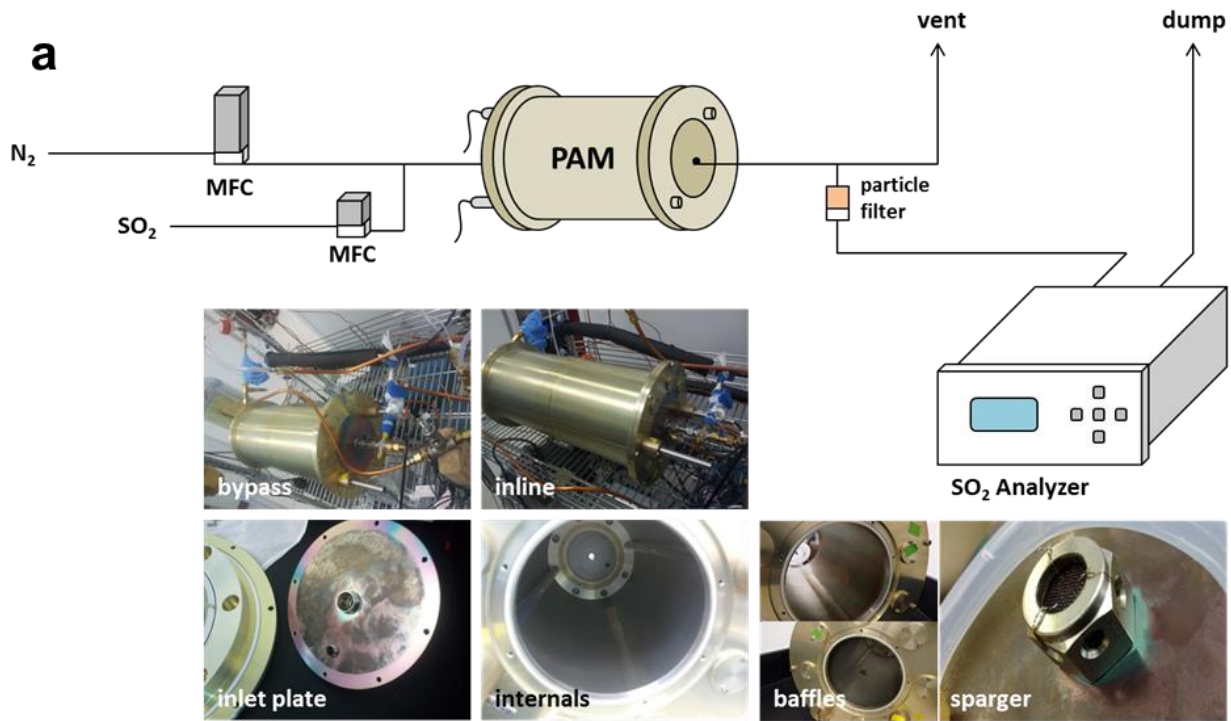
1034

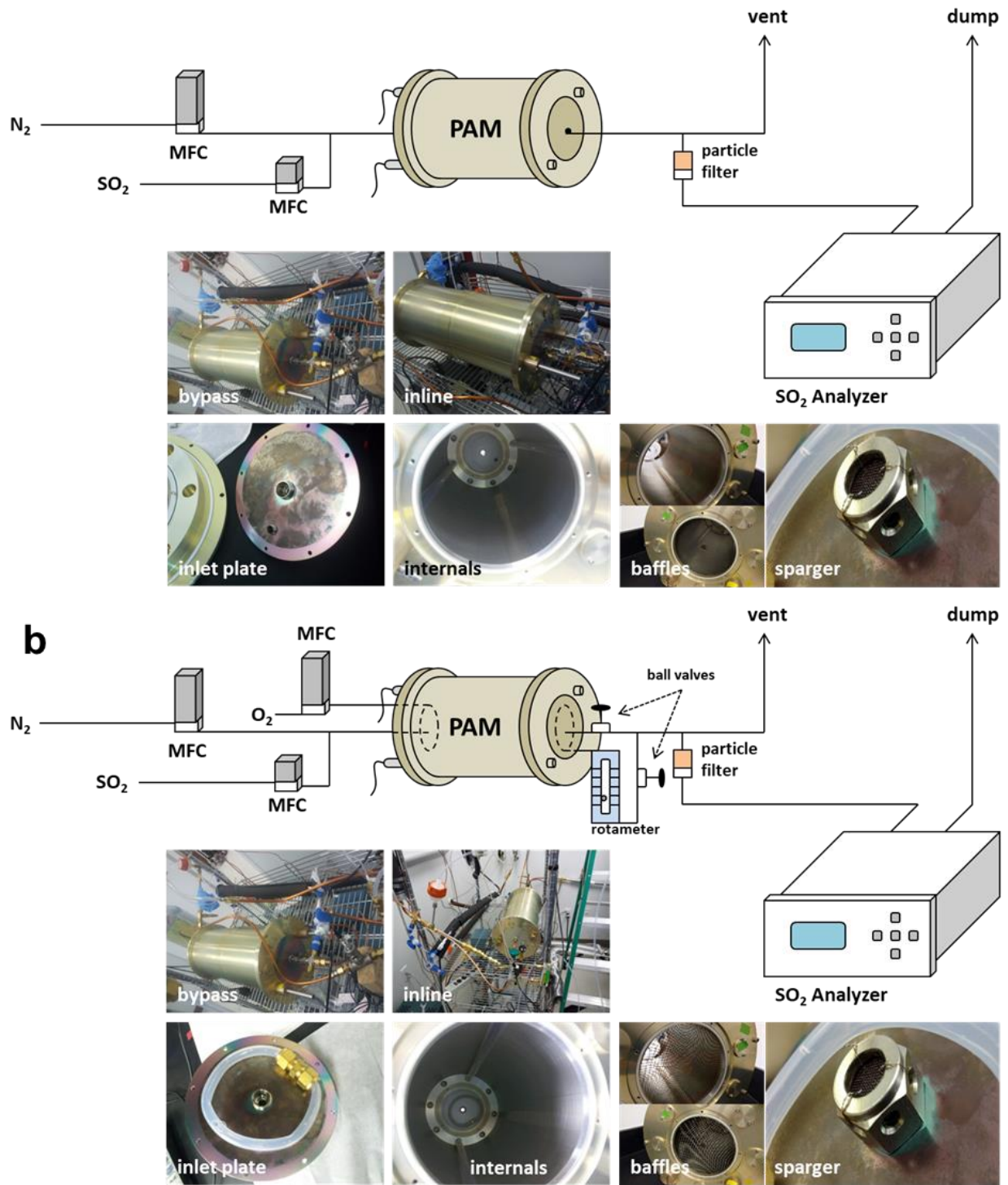
1035 We would like to express appreciation for the valuable discussions with Prof. Jay Turner, Prof.
1036 James Ballard, Christopher Oxford, David Hagan, and Tim Lee at Washington University in St.
1037 Louis, and valuable correspondence with Prof. William Brune at the Pennsylvania State University
1038 and Dr. Andrew Lambe at Aerodyne Research Inc. We would also like to thank ENGYS and Prof.
1039 Milorad Duduković's CREL resources, who provided the necessary computational power to run
1040 CFD. This work was partly funded by the National Science Foundation (NSF) CBET Award
1041 #1236865, and NSF CBET Award #1437933.

1042

1043 **Figures**

1044

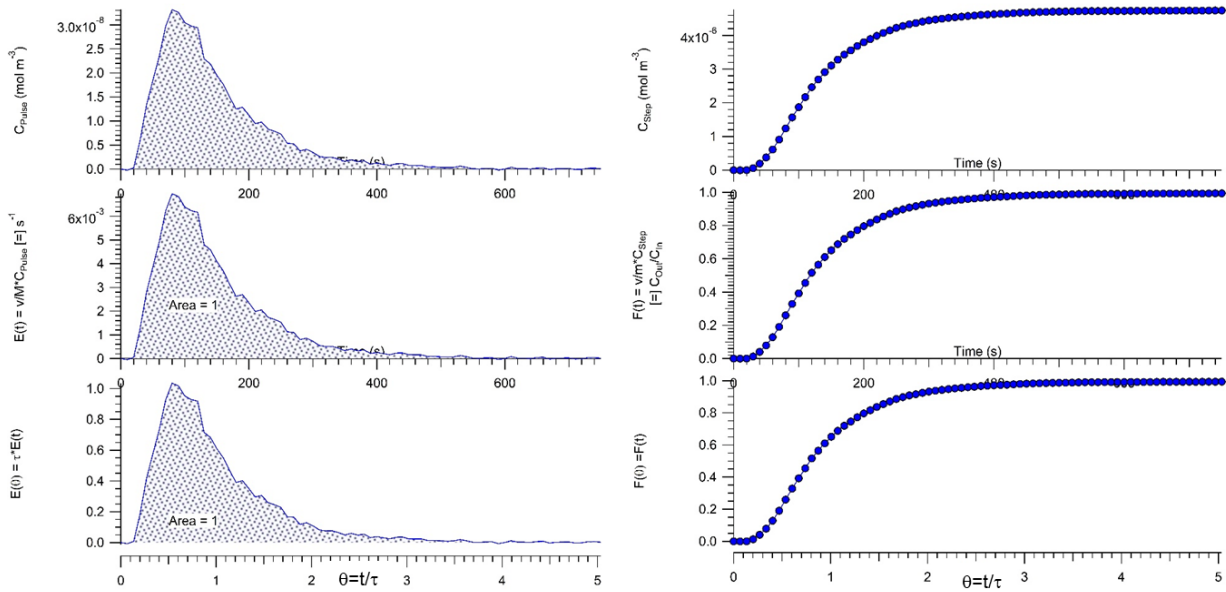




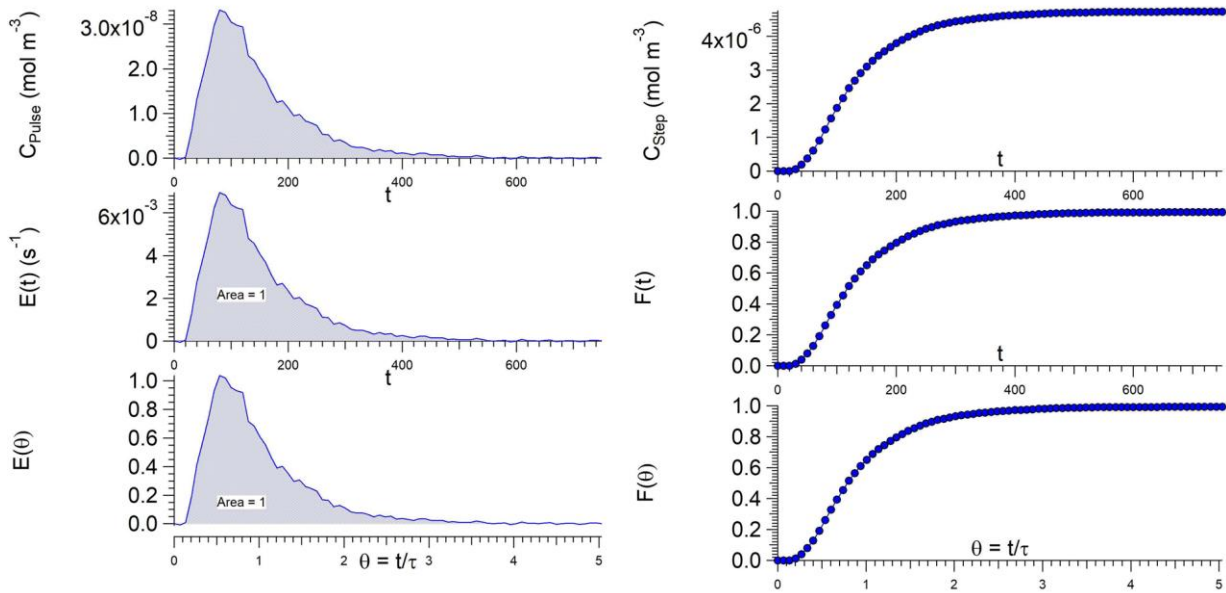
1046
 1047
 1048
 1049

Figure 1: Experimental setup for tracer studies for a) one inlet and one outlet and b) peripheral inlets and outlets. The main difference is the presence of the ring sparger in b).

1050



1051



1052

Figure 2: Tracer tests at 10 L min^{-1} (78s spacetime) through the reactor for configuration I. This figure serves as an illustrative example for non-dimensionalizing tracer response curves.

1053

1054

1055

1056

1057

1058

1059

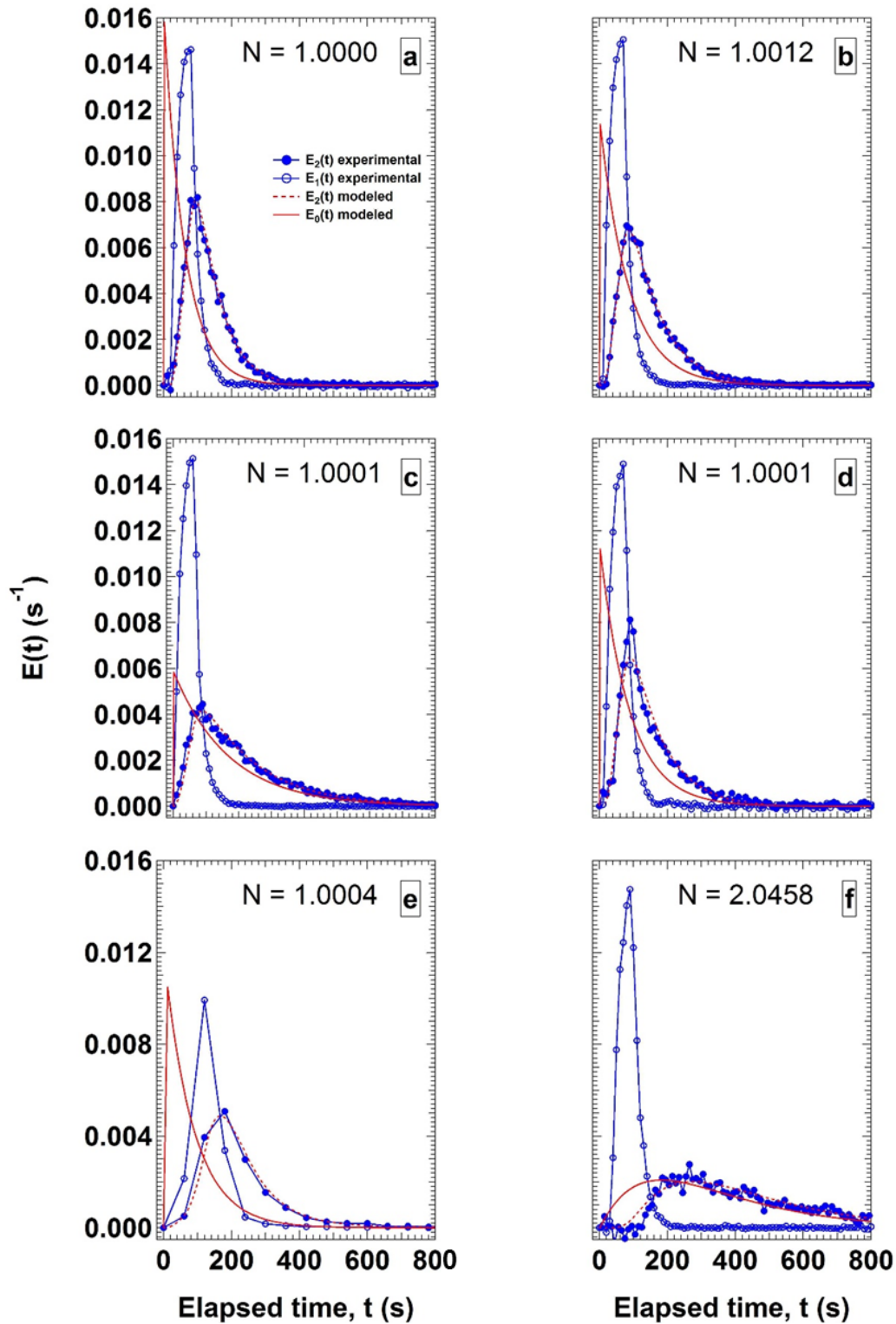
1060

1061

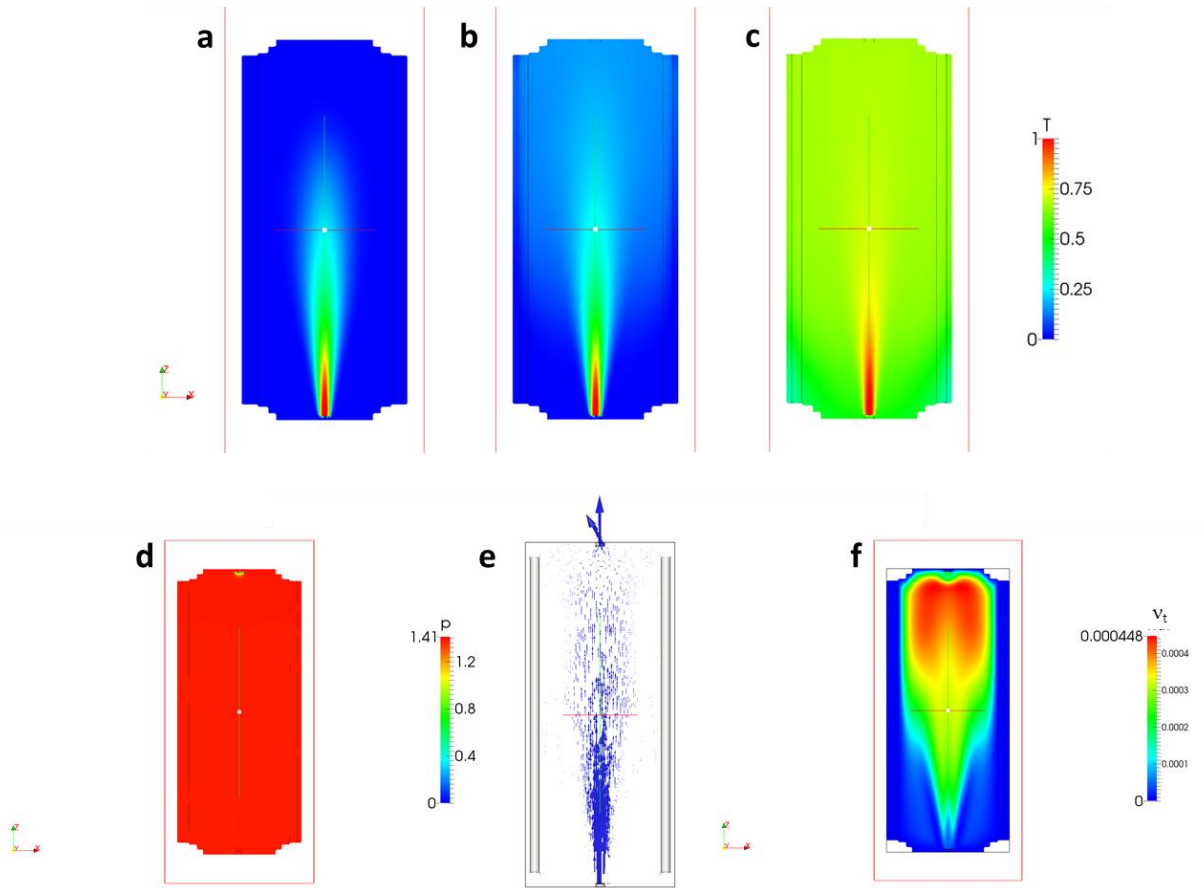
1062

1063

1064
1065
1066
1067
1068
1069
1070
1071
1072
1073
1074
1075
1076
1077
1078
1079
1080

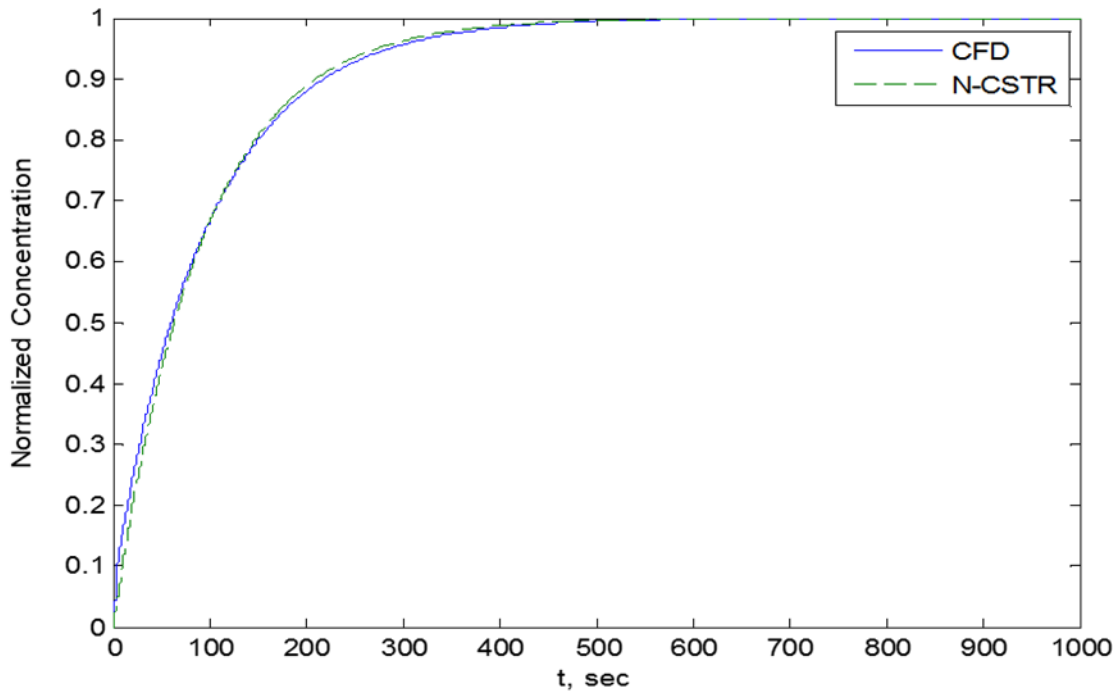
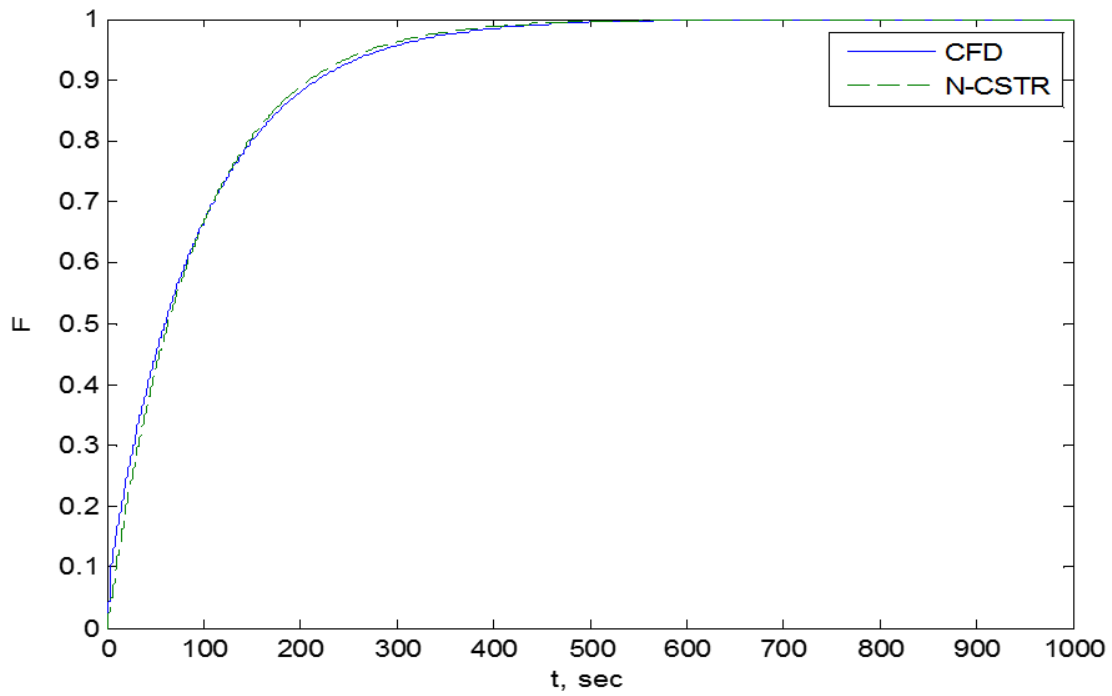


1081
 1082 Figure 3: E-Curves for the WU-PAM configuration I at a) 52s b) 78s c) 156s spacetimes, at 78s
 1083 spacetimes for d) configuration II e) configuration III, and f) for configuration IV at 411s
 1084 spacetime. Details on the configurations are in the Methods section. Lower frequency data for
 1085 panel e) was due to instrument repair, and temporarily set on longer averages.

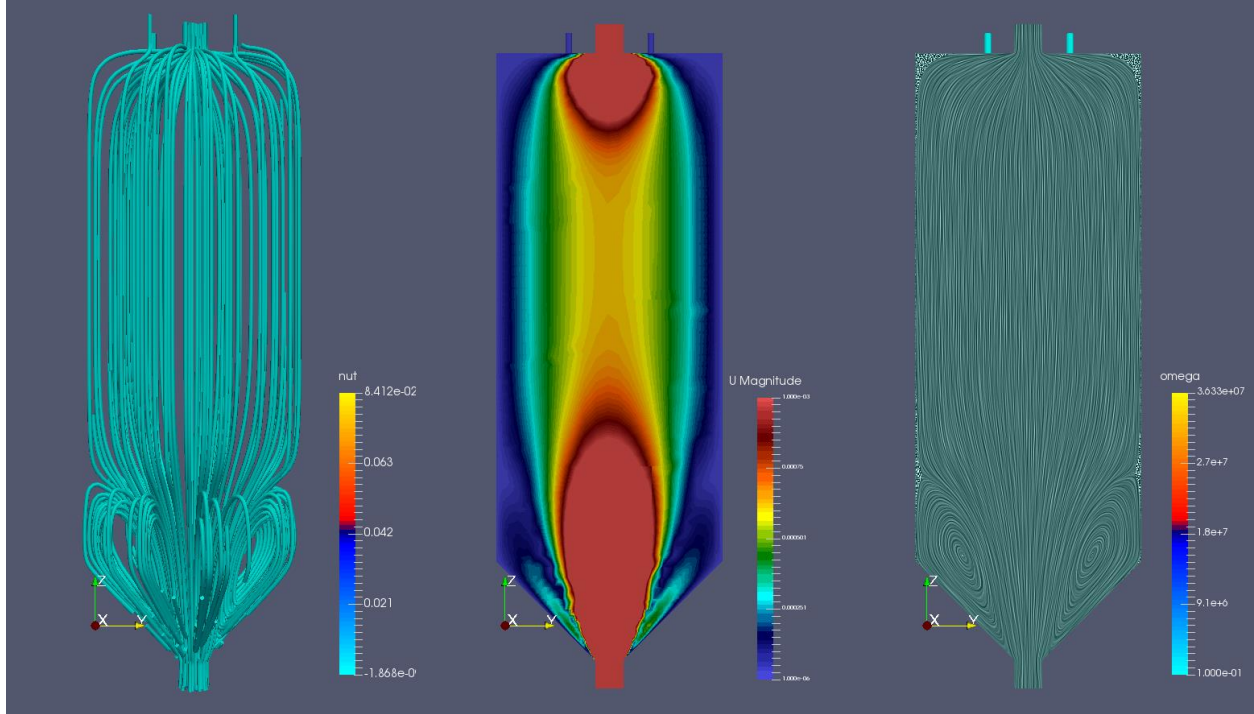


1086
 1087 Figure 4: CFD output for configuration I at 78s spacetime: snapshots at a) 1s b) 10s and c) 100s of
 1088 runtime, and d) pressure field, e) velocity (vector) field, and f) turbulent diffusivity field. Color
 1089 scales are dimensionless scalar concentration for the tracer (a-c), Bar for the pressure field (d), and
 1090 cSt for the kinematic viscosity (f).

1091
 1092
 1093
 1094
 1095
 1096
 1097
 1098
 1099
 1100
 1101
 1102
 1103
 1104
 1105



1106
 1107 Figure 5: Comparison of F-Curve output between simulation (CFD) and tracer test (N-CSTR) for
 1108 configuration I at 78s spacetime. N-CSTR is an acronym (describing 'N' CSTRs in series)
 1109 equivalent to TIS: both refer to the Tank-in-Series model (see Section 3.2).
 1110



1111
 1112 Figure 6: CFD analysis on the effect of inlet cone and peripheral outlets on fluid flow. All figures
 1113 represent a visualization of the flow field, with color scales representing (from left to right):
 1114 kinematic viscosity, velocity, and ω . The 3D representation on the leftmost figure highlights the
 1115 uniformity of the recirculation region.

1116 **Appendix A: The use of E-Curves and F-Curves**

1117

1118 To determine RTDs, we injected tracer in a steady stream rather than a single pulse. This prolonged
 1119 and constant injection, which we call a step input, gave us $F(t)$, from which we can derive $E(t)$ as
 1120 follows:

$$F(t) = \frac{v}{m} C_{step} \quad (A1)$$

$$E(t) = \frac{dF(t)}{dt}, \quad (A2)$$

1121 where v is the volumetric flowrate in m^3s^{-1} , m is the molar flowrate of the tracer in mol s^{-1} , and
 1122 C_{step} is the concentration of the tracer for a step input in mol m^{-3} . Therefore, $F(t)$ is dimensionless,
 1123 and $E(t)$ in this example has units of s^{-1} . The area under the E-Curve is unity, representing the PDF
 1124 of the system:

$$\int_0^{\infty} E(t)dt = 1. \quad (\text{A3})$$

1125 Similarly, for the dimensionless domain

$$\int_0^{\infty} E(\theta)d\theta = 1. \quad (\text{A4})$$

1126 And if we take \bar{t} to be the mean residence time of the reactor, then

$$\theta = \frac{t}{\bar{t}}. \quad (\text{A5})$$

1127 The additional utility of the dimensionless domain is that for reactors of different sizes, built to
 1128 behave the same, the RTD is numerically identical. For example, if PAM OFRs are operated in
 1129 different ways (e.g., they operate at different flowrates) or are built in different sizes but display
 1130 the same E-Curve in the dimensionless domain, then their performance will be identical, and their
 1131 mean residence time will always occur at $\theta = 1$. This identity would apply for the F-Curve as well
 1132 in both domains, where from Eq. (A2) we can see that

1133

$$F(t) = \int_0^t E(t)dt \quad (\text{A6})$$

$$F(\theta) = \int_0^t E(\theta)d\theta. \quad (\text{A7})$$

1134 The mathematical properties of interest for PDFs are their moments: These have quantitative
 1135 meanings in E-Curve analysis. A general equation for the moments of a function $f(x)$ is

$$\mu_n = \int_{-\infty}^{\infty} x^n \cdot f(x)dx, \quad (\text{A8})$$

1136 where μ_n is the nth moment of the distribution. If we consider a raw C(t) dataset from our tracer,
 1137 we can derive the moments:

$$\frac{\int_0^{\infty} C(t)dt}{\int_0^{\infty} C(t)dt} = \int_0^{\infty} E(t)dt = 1 = \mu_0 \quad (\text{A9})$$

$$\frac{\int_0^{\infty} t \cdot C(t) dt}{\int_0^{\infty} C(t) dt} = \int_0^{\infty} t \cdot E(t) dt = \bar{t} = \mu_1. \quad (\text{A10})$$

1138 Here, we are interested in the first moment, which represents the mean residence time. For higher
 1139 moments, we use the central moments of the distribution since we are interested in quantities like
 1140 variance, skewness, and kurtosis around the mean (and not around zero). This alters Eq. (A8) as
 1141 follows:

$$\mu_n = \int_{-\infty}^{\infty} (x - a)^n \cdot f(x) dx; n \geq 2, \quad (\text{A11})$$

1142 where a is a constant, and is generally the mean of the distribution (\bar{t} in this case). Thus, the second
 1143 (central) moment of the E-Curve becomes

$$\frac{\int_0^{\infty} (t - \bar{t})^2 \cdot C(t) dt}{\int_0^{\infty} C(t) dt} = \int_0^{\infty} (t - \bar{t})^2 \cdot E(t) dt = \sigma^2 = \quad (\text{A12})$$

$$\mu_2,$$

1144 where σ^2 has a clear physical meaning, and is the variance around the mean. Higher moments
 1145 (skewness and kurtosis) can be of use, and require additional math, but are not addressed in this
 1146 work.

1147

1148 **Appendix B: Algorithm for direct deconvolution**

1149

1150 Here, we perform an inverse operation to Eq. (7) (Sun, 2010) and work towards an output curve:

$$1151 \quad E_2(t) = \int_0^t E_1(t - t') E_0(t') dt'$$

1152 (B1)

1153 , where E_0 is the RTD of interest, E_1 is the RTD of another component in series with E_0 , and E_2 is
 1154 the convoluted RTD. The deconvolution task is to solve for E_0 with measured E_1 and E_2 . Due to

1155 the unknown function forms of E_1 and E_2 , the integral is most easily resolved numerically. Thus,
 1156 the time is discretized into $t_{i-1} \leq t \leq t_i$, where $t_i = i\Delta t, i = 0 \dots \infty$. The time interval Δt is
 1157 determined by the data acquisition frequency for E_1 and E_2 , and is small enough to resolve the
 1158 RTD's in fine detail. An even smaller Δt is also feasible by interpolating the data on the finer
 1159 temporal resolution. Eq. (B1) is now rewritten as (B2):

$$E_2(t_i) = \int_0^{t_i} E_1(t_i - t')E_0(t')dt' = \sum_{j=1}^i \int_{t_{j-1}}^{t_j} E_1(t_i - t')E_0(t')dt'$$

(B2)

1162 Within the small interval between t_{j-1} and t_j , we can assume E_1 and E_0 to be either constant (0th
 1163 order) or linear with time (1st order). Obviously the 1st order approximation is more accurate than
 1164 the 0th order with a little more complexity in the integration. Both methods have been tested and
 1165 proven to result in similar deconvoluted RTD, indicating that 0th order is good enough with
 1166 sufficiently small Δt . Thus the following derivation takes the 0th order simplification, i.e. for
 1167 $t_{j-1} \leq t' \leq t_j$:

$$\begin{aligned} E_1(t_i - t') &= \frac{1}{2} \left(E_1(t_i - t_{j-1}) + E_1(t_i - t_j) \right) = \frac{1}{2} \left(E_1(t_{i-j+1}) + E_1(t_{i-j}) \right) \\ &= \frac{1}{2} (E_1|_{i-j+1} + E_1|_{i-j}) \end{aligned}$$

(B3)

$$E_0(t') = \frac{1}{2} \left(E_0(t_{j-1}) + E_0(t_j) \right) = \frac{1}{2} (E_0|_{j-1} + E_0|_j)$$

(B4)

1173 , which are Eq. (B3) and (B4) with simplified notation (e.g. from $E_0(t_j)$ to $E_0|_j$). Thus Eq. (B5):

$$\int_{t_{j-1}}^{t_j} E_1(t_i - t')E_0(t')dt' = \frac{1}{4} (E_1|_{i-j+1} + E_1|_{i-j})(E_0|_{j-1} + E_0|_j)\Delta t$$

1175 (B5)

1176 Eq. (B2) becomes (B6):

$$1177 \quad E_2|_i = \sum_{j=1}^i \frac{\Delta t}{4} (E_1|_{i-j+1} + E_1|_{i-j})(E_0|_{j-1} + E_0|_j)$$

1178 (B6)

1179 , where i starts at 1 as $E_2|_0 = E_1|_0 = E_0|_0 = 0$ (except for RTD of an ideal CSTR). Again, E_2 and
1180 E_1 are known by measurements, and E_0 is the unknown to be solved. Let x be
1181 $[E_0|_1, E_0|_2, \dots, E_0|_n]$, where n is an integer sufficiently large beyond which E_0 is considered to
1182 have converged to zero. Let

$$1183 \quad a_{i,j} = \frac{\Delta t}{4} (E_1|_{i-j+1} + E_1|_{i-j})$$

1184 (B7)

$$1185 \quad E_2|_1 - a_{1,1}E_0|_0 = a_{1,1}E_0|_1$$

$$1186 \quad E_2|_2 - a_{2,1}E_0|_0 = (a_{2,1} + a_{2,2})E_0|_1 + a_{2,2}E_0|_2$$

$$1187 \quad E_2|_3 - a_{3,1}E_0|_0 = (a_{3,1} + a_{3,2})E_0|_1 + (a_{3,2} + a_{3,3})E_0|_2 + a_{3,3}E_0|_3$$

1188 ...

1189 Therefore, define the coefficient matrix A in Eq. (B8) where

$$1190 \quad A_{i,j} = \begin{cases} a_{i,i} & \text{if } j = i \\ a_{i,j} + a_{i,j+1} & \text{if } j < i \\ 0 & \text{if } j > i \end{cases}$$

1191 (B8)

1192 And define the vector b in Eq. (B9) where

$$1193 \quad b_i = E_2|_i - a_{i,1}E_0|_0$$

1194 (B9)

1195 In this way, the integral Eq. (B1) is converted to a linear algebra problem in Eq. (B10):

$$1196 \quad \quad \quad Ax = b$$

1197 (B10)

1198 Therefore, E_0 can be obtained by solving

$$1199 \quad \quad \quad x = A^{-1}b$$

1200 (B11)

1201 This is called “direct deconvolution” which requires taking inverse of the coefficient matrix A .
1202 However, in some cases A is ill conditioned and numerical inversion method like “inv(A)” in
1203 MATLAB does not converge. This non-ideality results primarily from measurement uncertainties.
1204 Thus, instead of directly solving Eq. (B10), it is proposed in this work to first assume a reasonable
1205 function form for x , e.g. the tanks-in-series (TIS) model, and then iteratively update the model
1206 parameters to minimize the residual of Eq. (B10). This “indirect deconvolution” method always
1207 works to yield a stable and accurate solution of E_0 , the accuracy being judged by comparing b and
1208 $b' = Ax'$, where x' represents the converged solution. The validity of the “indirect deconvolution”
1209 depends on the reactor model being assumed. The TIS model is one of the two mostly used non-
1210 ideal reactor models (the other one is the axial dispersion model), which has proven to work well
1211 for the PAM reactor under investigation. The model parameter N (the number of CSTR’s)
1212 indicates the non-ideality of the reactor, i.e. the larger N is than 1, the more differently the reactor
1213 behaves from an ideal CSTR. The mathematical form of the TIS model can be found in Section
1214 3.2.

1215

1216

$$E_z(t) = \int_0^t E_x(t-t') \cdot E_0(t') dt' \quad (B1)$$

1217 In discrete form, taking a constant time step Δt , we can take a datapoint at $t_i = i\Delta t$,

$$E_{z_N}(t_i) = \sum_{t'=1}^N \int_{t_{i-1}}^{t_i} E_{\pm}(t_N - t') \cdot E_{\mp}(t') dt' \quad (\text{B2})$$

1218 If we then assume that the functions $E_{\pm}(t - t')$ and $E_{\mp}(t')$ are constant for the interval $t_{i-1} \leq t' \leq$
 1219 t_i , we can simplify the integral:

$$E_{\pm}(t_N - t') = \frac{1}{2}(E_{\pm}|_{N-1} + E_{\pm}|_{N-i+1}) \quad (\text{B3})$$

$$E_{\mp}(t') = \frac{1}{2}(E_{\mp}|_i + E_{\mp}|_{i-1}) \quad (\text{B4})$$

$$\int_{t_{i-1}}^{t_i} E_{\pm}(t_N - t') \cdot E_{\mp}(t') dt' = \frac{1}{4}(E_{\pm}|_{N-1} + E_{\pm}|_{N-i+1})(E_{\mp}|_i + E_{\mp}|_{i-1})\Delta t \quad (\text{B5})$$

1220 Now, Eq. (B2) becomes

$$E_{z_N}(t_i) = \sum_{t'=1}^N \frac{1}{4}(E_{\pm}|_{N-1} + E_{\pm}|_{N-i+1})(E_{\mp}|_i + E_{\mp}|_{i-1})\Delta t \quad (\text{B6})$$

1221 From experimental data, we can accurately collect datapoints for $(E_{\pm}|_{N-1} + E_{\pm}|_{N-i+1})$ as well as
 1222 $E_{z}(t_i)$, so we need to rearrange for $(E_{\mp}|_i + E_{\mp}|_{i-1})$, which has to be solved numerically in matrix
 1223 form. Let

$$\alpha_i = \beta_i = \frac{1}{4}(E_{\pm}|_{N-1} + E_{\pm}|_{N-i+1}) \quad (\text{B7})$$

$$A_{N,i} = \begin{cases} \alpha_i + \beta_{i+1} & i = 1, 2, \dots, (N-1) \\ \alpha_N & i = N \end{cases} \quad (\text{B8})$$

1224 Upon the initial condition

$$B_N = \frac{E_z(t_N)}{\Delta t} - \beta_N E_{\mp}|_0, \quad (\text{B9})$$

1225 we have that

$$B_N = \sum_{i=1}^N A_{N,i} E_{\mp}|_i \quad (\text{B10})$$

1226 Finally,

$$\vec{E}_0(t) = \vec{A}^{-1} \vec{B}. \quad (\text{B11})$$

1227

1228 References

1229

1230 Aris, R.: On the Dispersion of a Solute in a Fluid Flowing through a Tube, Proc. R. Soc. Math.
1231 Phys. Eng. Sci., 235(1200), 67–77, doi:10.1098/rspa.1956.0065, 1956.

1232 Bourne, J. R.: Mixing and the Selectivity of Chemical Reactions, Org. Process Res. Dev., 7(4),
1233 471–508, doi:10.1021/op020074q, 2003.

1234 Brune, W. H., Schwab, J. J. and Anderson, J. G.: Laser magnetic resonance, resonance
1235 fluorescence, resonance absorption studies of the reaction kinetics of O + OH -> H + O₂, O + HO₂
1236 -> OH + O₂, N + OH -> H + NO, N + HO₂ -> products at 300 K between 1 and 5 torr, J. Phys.
1237 Chem., 87(22), 4503–4514, doi:10.1021/j100245a034, 1983.

1238 Bruns, E. A., El Haddad, I., Keller, A., Klein, F., Kumar, N. K., Pieber, S. M., Corbin, J. C.,
1239 Slowik, J. G., Brune, W. H., Baltensperger, U. and Prévôt, A. S. H.: Inter-comparison of laboratory
1240 smog chamber and flow reactor systems on organic aerosol yield and composition, Atmospheric
1241 Meas. Tech., 8(6), 2315–2332, doi:10.5194/amt-8-2315-2015, 2015.

1242 Canagaratna, M. R., Jayne, J. T., Jimenez, J. L., Allan, J. D., Alfarra, M. R., Zhang, Q., Onasch,
1243 T. B., Drewnick, F., Coe, H., Middlebrook, A., Delia, A., Williams, L. R., Trimborn, A. M.,
1244 Northway, M. J., DeCarlo, P. F., Kolb, C. E., Davidovits, P. and Worsnop, D. R.: Chemical and
1245 microphysical characterization of ambient aerosols with the aerodyne aerosol mass spectrometer,
1246 Mass Spectrom. Rev., 26(2), 185–222, doi:10.1002/mas.20115, 2007.

1247 Cazorla, M. and Brune, W. H.: Measurement of Ozone Production Sensor, Atmospheric Meas.
1248 Tech., 3(3), 545–555, doi:10.5194/amt-3-545-2010, 2010.

1249 Chhabra, P. S., Lambe, A. T., Canagaratna, M. R., Stark, H., Jayne, J. T., Onasch, T. B.,
1250 Davidovits, P., Kimmel, J. R. and Worsnop, D. R.: Application of high-resolution time-of-flight
1251 chemical ionization mass spectrometry measurements to estimate volatility distributions of α -
1252 pinene and naphthalene oxidation products, Atmospheric Meas. Tech., 8(1), 1–18,
1253 doi:10.5194/amt-8-1-2015, 2015.

1254 Claeys, M.: Formation of Secondary Organic Aerosols Through Photooxidation of Isoprene,
1255 Science, 303(5661), 1173–1176, doi:10.1126/science.1092805, 2004.

1256 Crouse, J. D., McKinney, K. A., Kwan, A. J. and Wennberg, P. O.: Measurement of Gas-Phase
1257 Hydroperoxides by Chemical Ionization Mass Spectrometry, Anal. Chem., 78(19), 6726–6732,
1258 doi:10.1021/ac0604235, 2006.

1259 [Crump, J. G. and Seinfeld, J. H.: Aerosol behavior in the continuous stirred tank reactor, *AIChE*](#)
1260 [*J.*, 26\(4\), 610–616, doi:10.1002/aic.690260412, 1980.](#)

1261 [Crump, J. G., Flagan, R. C. and Seinfeld, J. H.: Particle Wall Loss Rates in Vessels, *Aerosol Sci.*](#)
1262 [*Technol.*, 2\(3\), 303–309, doi:10.1080/02786828308958636, 1982.](#)

1263 [Danckwerts, P. V.: Continuous flow systems, *Chem. Eng. Sci.*, 2\(1\), 1–13, doi:10.1016/0009-](#)
1264 [*2509\(53\)80001-1*, 1953.](#)

1265 [Deckwer, W.-D.: Non-isobaric bubble columns with variable gas velocity, *Chem. Eng. Sci.*, 31\(4\),](#)
1266 [309–317, doi:10.1016/0009-2509\(76\)85076-2, 1976.](#)

1267 [Ezell, M. J., Johnson, S. N., Yu, Y., Perraud, V., Bruns, E. A., Alexander, M. L., Zelenyuk, A.,](#)
1268 [Dabdub, D. and Finlayson-Pitts, B. J.: A New Aerosol Flow System for Photochemical and](#)
1269 [Thermal Studies of Tropospheric Aerosols, *Aerosol Sci. Technol.*, 44\(5\), 329–338,](#)
1270 [doi:10.1080/02786821003639700, 2010.](#)

1271 [Fogler, H. S.: Elements of chemical reaction engineering, 4th ed., Prentice Hall PTR, Upper Saddle](#)
1272 [River, NJ., 2006.](#)

1273 [George, I. J. and Abbatt, J. P. D.: Chemical evolution of secondary organic aerosol from OH-](#)
1274 [initiated heterogeneous oxidation, *Atmospheric Chem. Phys.*, 10\(12\), 5551–5563,](#)
1275 [doi:10.5194/acp-10-5551-2010, 2010.](#)

1276 [George, I. J., Vlasenko, A., Slowik, J. G., Broekhuizen, K. and Abbatt, J. P. D.: Heterogeneous](#)
1277 [oxidation of saturated organic aerosols by hydroxyl radicals: uptake kinetics, condensed-phase](#)
1278 [products, and particle size change, *Atmospheric Chem. Phys.*, 7\(16\), 4187–4201, doi:10.5194/acp-](#)
1279 [*7-4187-2007*, 2007.](#)

1280 [de Gouw, J. and Warneke, C.: Measurements of volatile organic compounds in the earth’s](#)
1281 [atmosphere using proton-transfer-reaction mass spectrometry, *Mass Spectrom. Rev.*, 26\(2\), 223–](#)
1282 [257, doi:10.1002/mas.20119, 2007.](#)

1283 [Haagen-Smit, A. J.: Chemistry and Physiology of Los Angeles Smog, *Ind. Eng. Chem.*, 44\(6\),](#)
1284 [1342–1346, doi:10.1021/ie50510a045, 1952.](#)

1285 [Haagen-Smit, A. J.: Photochemistry and Smog, *J. Air Pollut. Control Assoc.*, 13\(9\), 444–454,](#)
1286 [doi:10.1080/00022470.1963.10468205, 1963.](#)

1287 [Haagen-Smit, A. J.: A Lesson from the Smog Capital of the World, *Proc. Natl. Acad. Sci.*, 67\(2\),](#)
1288 [887–897, doi:10.1073/pnas.67.2.887, 1970.](#)

1289 [Hamed, M.: Hydrodynamics, Mixing, and Mass Transfer in Bubble Columns with Internals, PhD,](#)
1290 [Washington University in St. Louis, Saint Louis., 2012.](#)

1291 [Han, L.: Hydrodynamics, back-mixing, and mass transfer in a slurry bubble column reactor for](#)
1292 [Fischer-Tropsch alternative fuels, DSc, Washington University in St. Louis, Saint Louis., 2007.](#)

1293 [Hansel, A., Jordan, A., Holzinger, R., Prazeller, P., Vogel, W. and Lindinger, W.: Proton transfer](#)
1294 [reaction mass spectrometry: on-line trace gas analysis at the ppb level, Int. J. Mass Spectrom. Ion](#)
1295 [Process., 149–150, 609–619, doi:10.1016/0168-1176\(95\)04294-U, 1995.](#)

1296 [Howard, C. J.: Kinetic measurements using flow tubes, J. Phys. Chem., 83\(1\), 3–9,](#)
1297 [doi:10.1021/j100464a001, 1979.](#)

1298 [Huang, Y., Coggon, M. M., Zhao, R., Lignell, H., Bauer, M. U., Flagan, R. C. and Seinfeld, J. H.:](#)
1299 [The Caltech Photooxidation Flow Tube Reactor – I: Design and Fluid Dynamics,](#)
1300 [Atmospheric Meas. Tech. Discuss., 1–36, doi:10.5194/amt-2016-282, 2016.](#)

1301 [Jayne, J. T., Leard, D. C., Zhang, X., Davidovits, P., Smith, K. A., Kolb, C. E. and Worsnop, D.](#)
1302 [R.: Development of an Aerosol Mass Spectrometer for Size and Composition Analysis of](#)
1303 [Submicron Particles, Aerosol Sci. Technol., 33\(1–2\), 49–70, doi:10.1080/027868200410840,](#)
1304 [2000.](#)

1305 [Kamens, R. M., Gery, M. W., Jeffries, H. E., Jackson, M. and Cole, E. I.: Ozone-isoprene](#)
1306 [reactions: Product formation and aerosol potential, Int. J. Chem. Kinet., 14\(9\), 955–975,](#)
1307 [doi:10.1002/kin.550140902, 1982.](#)

1308 [Kang, E., Root, M. J., Toohey, D. W. and Brune, W. H.: Introducing the concept of Potential](#)
1309 [Aerosol Mass \(PAM\), Atmospheric Chem. Phys., 7\(22\), 5727–5744, doi:10.5194/acp-7-5727-](#)
1310 [2007, 2007.](#)

1311 [Kang, E., Toohey, D. W. and Brune, W. H.: Dependence of SOA oxidation on organic aerosol](#)
1312 [mass concentration and OH exposure: experimental PAM chamber studies, Atmospheric Chem.](#)
1313 [Phys., 11\(4\), 1837–1852, doi:10.5194/acp-11-1837-2011, 2011.](#)

1314 [Katrib, Y., Biskos, G., Buseck, P. R., Davidovits, P., Jayne, J. T., Mochida, M., Wise, M. E.,](#)
1315 [Worsnop, D. R. and Martin, S. T.: Ozonolysis of Mixed Oleic-Acid/Stearic-Acid Particles:](#)
1316 [Reaction Kinetics and Chemical Morphology, J. Phys. Chem. A, 109\(48\), 10910–10919,](#)
1317 [doi:10.1021/jp054714d, 2005.](#)

1318 [Keller, A. and Burtscher, H.: A continuous photo-oxidation flow reactor for a defined](#)
1319 [measurement of the SOA formation potential of wood burning emissions, J. Aerosol Sci., 49, 9–](#)
1320 [20, doi:10.1016/j.jaerosci.2012.02.007, 2012.](#)

1321 [Kessler, S. H., Smith, J. D., Che, D. L., Worsnop, D. R., Wilson, K. R. and Kroll, J. H.: Chemical](#)
1322 [Sinks of Organic Aerosol: Kinetics and Products of the Heterogeneous Oxidation of Erythritol and](#)
1323 [Levoglucosan, Environ. Sci. Technol., 44\(18\), 7005–7010, doi:10.1021/es101465m, 2010.](#)

1324 [Kessler, S. H., Nah, T., Daumit, K. E., Smith, J. D., Leone, S. R., Kolb, C. E., Worsnop, D. R.,](#)
1325 [Wilson, K. R. and Kroll, J. H.: OH-Initiated Heterogeneous Aging of Highly Oxidized Organic](#)
1326 [Aerosol, J. Phys. Chem. A, 116\(24\), 6358–6365, doi:10.1021/jp212131m, 2012.](#)

1327 [Keyser, L. F.: Absolute rate constant of the reaction OH + H₂O₂ -> HO₂ + H₂O from 245 to 423](#)
1328 [K, J. Phys. Chem., 84\(13\), 1659–1663, doi:10.1021/j100450a001, 1980.](#)

1329 [Keyser, L. F.: High-pressure flow kinetics. A study of the hydroxyl + hydrogen chloride reaction](#)
1330 [from 2 to 100 torr, J. Phys. Chem., 88\(20\), 4750–4758, doi:10.1021/j150664a061, 1984.](#)

1331 [Knopf, D. A., Anthony, L. M. and Bertram, A. K.: Reactive Uptake of O₃ by Multicomponent and](#)
1332 [Multiphase Mixtures Containing Oleic Acid, J. Phys. Chem. A, 109\(25\), 5579–5589,](#)
1333 [doi:10.1021/jp0512513, 2005.](#)

1334 [Kroll, J. H. and Seinfeld, J. H.: Chemistry of secondary organic aerosol: Formation and evolution](#)
1335 [of low-volatility organics in the atmosphere, Atmos. Environ., 42\(16\), 3593–3624,](#)
1336 [doi:10.1016/j.atmosenv.2008.01.003, 2008.](#)

1337 [Kroll, J. H., Ng, N. L., Murphy, S. M., Flagan, R. C. and Seinfeld, J. H.: Secondary Organic](#)
1338 [Aerosol Formation from Isoprene Photooxidation, Environ. Sci. Technol., 40\(6\), 1869–1877,](#)
1339 [doi:10.1021/es0524301, 2006.](#)

1340 [Kroll, J. H., Smith, J. D., Worsnop, D. R. and Wilson, K. R.: Characterisation of lightly oxidised](#)
1341 [organic aerosol formed from the photochemical aging of diesel exhaust particles, Environ. Chem.,](#)
1342 [9\(3\), 211, doi:10.1071/EN11162, 2012.](#)

1343 [Lamb, J. J., Molina, L. T., Smith, C. A. and Molina, M. J.: Rate constant of the hydroxy radical +](#)
1344 [hydrogen peroxide .fwdarw. hydroperoxo radical + water reaction, J. Phys. Chem., 87\(22\), 4467–](#)
1345 [4470, doi:10.1021/j100245a028, 1983.](#)

1346 [Lambe, A., Massoli, P., Zhang, X., Canagaratna, M., Nowak, J., Daube, C., Yan, C., Nie, W.,](#)
1347 [Onasch, T., Jayne, J., Kolb, C., Davidovits, P., Worsnop, D. and Brune, W.: Controlled nitric oxide](#)
1348 [production via O\(1D\) + N₂O reactions for use in oxidation flow reactor studies, Atmospheric](#)
1349 [Meas. Tech., 10\(6\), 2283–2298, doi:10.5194/amt-10-2283-2017, 2017.](#)

1350 [Lambe, A. T., Ahern, A. T., Williams, L. R., Slowik, J. G., Wong, J. P. S., Abbatt, J. P. D., Brune,](#)
1351 [W. H., Ng, N. L., Wright, J. P., Croasdale, D. R., Worsnop, D. R., Davidovits, P. and Onasch, T.](#)
1352 [B.: Characterization of aerosol photooxidation flow reactors: heterogeneous oxidation, secondary](#)
1353 [organic aerosol formation and cloud condensation nuclei activity measurements, Atmospheric](#)
1354 [Meas. Tech., 4\(3\), 445–461, doi:10.5194/amt-4-445-2011, 2011a.](#)

1355 [Lambe, A. T., Onasch, T. B., Massoli, P., Croasdale, D. R., Wright, J. P., Ahern, A. T., Williams,](#)
1356 [L. R., Worsnop, D. R., Brune, W. H. and Davidovits, P.: Laboratory studies of the chemical](#)
1357 [composition and cloud condensation nuclei \(CCN\) activity of secondary organic aerosol \(SOA\)](#)
1358 [and oxidized primary organic aerosol \(OPOA\), Atmospheric Chem. Phys. Discuss., 11\(5\), 13617–](#)
1359 [13653, doi:10.5194/acpd-11-13617-2011, 2011b.](#)

1360 [Lambe, A. T., Onasch, T. B., Croasdale, D. R., Wright, J. P., Martin, A. T., Franklin, J. P., Massoli,](#)
1361 [P., Kroll, J. H., Canagaratna, M. R., Brune, W. H., Worsnop, D. R. and Davidovits, P.: Transitions](#)
1362 [from Functionalization to Fragmentation Reactions of Laboratory Secondary Organic Aerosol](#)
1363 [\(SOA\) Generated from the OH Oxidation of Alkane Precursors, Environ. Sci. Technol., 46\(10\),](#)
1364 [5430–5437, doi:10.1021/es300274t, 2012.](#)

1365 [Lambe, A. T., Cappa, C. D., Massoli, P., Onasch, T. B., Forestieri, S. D., Martin, A. T., Cummings,](#)
1366 [M. J., Croasdale, D. R., Brune, W. H., Worsnop, D. R. and Davidovits, P.: Relationship between](#)

1367 [Oxidation Level and Optical Properties of Secondary Organic Aerosol, Environ. Sci. Technol.,](#)
1368 [130606090408002, doi:10.1021/es401043j, 2013.](#)

1369 [Lambe, A. T., Chhabra, P. S., Onasch, T. B., Brune, W. H., Hunter, J. F., Kroll, J. H., Cummings,](#)
1370 [M. J., Brogan, J. F., Parmar, Y., Worsnop, D. R., Kolb, C. E. and Davidovits, P.: Effect of oxidant](#)
1371 [concentration, exposure time, and seed particles on secondary organic aerosol chemical](#)
1372 [composition and yield, Atmospheric Chem. Phys., 15\(6\), 3063–3075, doi:10.5194/acp-15-3063-](#)
1373 [2015, 2015.](#)

1374 [Leone, J. A., Flagan, R. C., Grosjean, D. and Seinfeld, J. H.: An outdoor smog chamber and](#)
1375 [modeling study of toluene-NO_x photooxidation, Int. J. Chem. Kinet., 17\(2\), 177–216,](#)
1376 [doi:10.1002/kin.550170206, 1985.](#)

1377 [Levenspiel, O.: Chemical reaction engineering, 3rd ed., Wiley, New York., 1999.](#)

1378 [Levenspiel, O.: The chemical reactor omnibook, OSU Book Stores, Corvallis, Or., 2002.](#)

1379 [Li, R., Palm, B. B., Ortega, A. M., Hlywiak, J., Hu, W., Peng, Z., Day, D. A., Knote, C., Brune,](#)
1380 [W. H., de Gouw, J. A. and Jimenez, J. L.: Modeling the Radical Chemistry in an Oxidation Flow](#)
1381 [Reactor: Radical Formation and Recycling, Sensitivities, and the OH Exposure Estimation](#)
1382 [Equation, J. Phys. Chem. A, 119\(19\), 4418–4432, doi:10.1021/jp509534k, 2015.](#)

1383 [Liu, P. F., Abdelmalki, N., Hung, H.-M., Wang, Y., Brune, W. H. and Martin, S. T.: Ultraviolet](#)
1384 [and visible complex refractive indices of secondary organic material produced by photooxidation](#)
1385 [of the aromatic compounds toluene and m-xylene, Atmospheric Chem. Phys., 15\(3\), 1435–1446,](#)
1386 [doi:10.5194/acp-15-1435-2015, 2015.](#)

1387 [MacMullin, R. B. and Weber Jr., M.: The theory of short-circuiting in continuous-flow mixing](#)
1388 [vessels in series and the kinetics of chemical reactions in such systems, Trans. Am. Inst. Chem.](#)
1389 [Eng., 31, 409–458, 1935.](#)

1390 [Massoli, P., Lambe, A. T., Ahern, A. T., Williams, L. R., Ehn, M., Mikkilä, J., Canagaratna, M.](#)
1391 [R., Brune, W. H., Onasch, T. B., Jayne, J. T., Petäjä, T., Kulmala, M., Laaksonen, A., Kolb, C. E.,](#)
1392 [Davidovits, P. and Worsnop, D. R.: Relationship between aerosol oxidation level and hygroscopic](#)
1393 [properties of laboratory generated secondary organic aerosol \(SOA\) particles:](#)
1394 [HYGROSCOPICITY OF LABORATORY SOA, Geophys. Res. Lett., 37\(24\), n/a-n/a,](#)
1395 [doi:10.1029/2010GL045258, 2010.](#)

1396 [McNeill, V. F., Yatavelli, R. L. N., Thornton, J. A., Stipe, C. B. and Landgrebe, O.: Heterogeneous](#)
1397 [OH oxidation of palmitic acid in single component and internally mixed aerosol particles:](#)
1398 [vaporization and the role of particle phase, Atmospheric Chem. Phys., 8\(17\), 5465–5476,](#)
1399 [doi:10.5194/acp-8-5465-2008, 2008.](#)

1400 [Mills, P. L. and Duduković, M. P.: Deconvolution of noisy tracer response data by a linear filtering](#)
1401 [method, AIChE J., 34\(10\), 1752–1756, doi:10.1002/aic.690341025, 1988.](#)

1402 [Nozière, B., Barnes, I. and Becker, K.-H.: Product study and mechanisms of the reactions of \$\alpha\$ -](#)
1403 [pinene and of pinonaldehyde with OH radicals, J. Geophys. Res., 104\(D19\), 23645,](#)
1404 [doi:10.1029/1999JD900778, 1999.](#)

1405 [Ortega, A. M., Day, D. A., Cubison, M. J., Brune, W. H., Bon, D., de Gouw, J. A. and Jimenez, J.](#)
1406 [L.: Secondary organic aerosol formation and primary organic aerosol oxidation from biomass-](#)
1407 [burning smoke in a flow reactor during FLAME-3, Atmospheric Chem. Phys., 13\(22\), 11551–](#)
1408 [11571, doi:10.5194/acp-13-11551-2013, 2013.](#)

1409 [Ortega, A. M., Hayes, P. L., Peng, Z., Palm, B. B., Hu, W., Day, D. A., Li, R., Cubison, M. J.,](#)
1410 [Brune, W. H., Graus, M., Warneke, C., Gilman, J. B., Kuster, W. C., de Gouw, J., Gutiérrez-](#)
1411 [Montes, C. and Jimenez, J. L.: Real-time measurements of secondary organic aerosol formation](#)
1412 [and aging from ambient air in an oxidation flow reactor in the Los Angeles area, Atmospheric](#)
1413 [Chem. Phys., 16\(11\), 7411–7433, doi:10.5194/acp-16-7411-2016, 2016.](#)

1414 [Palm, B. B., Campuzano-Jost, P., Day, D. A., Ortega, A. M., Fry, J. L., Brown, S. S., Zarzana, K.](#)
1415 [J., Dube, W., Wagner, N. L., Draper, D. C., Kaser, L., Jud, W., Karl, T., Hansel, A., Gutiérrez-](#)
1416 [Montes, C. and Jimenez, J. L.: Secondary organic aerosol formation from in situ OH, O₃, and NO₃](#)
1417 [oxidation of ambient forest air in an oxidation flow reactor, Atmospheric Chem. Phys., 17\(8\),](#)
1418 [5331–5354, doi:10.5194/acp-17-5331-2017, 2017.](#)

1419 [Palm, B. B., de Sá, S. S., Day, D. A., Campuzano-Jost, P., Hu, W., Seco, R., Sjostedt, S. J., Park,](#)
1420 [J.-H., Guenther, A. B., Kim, S., Brito, J., Wurm, F., Artaxo, P., Thalman, R., Wang, J., Yee, L. D.,](#)
1421 [Wernis, R., Isaacman-VanWertz, G., Goldstein, A. H., Liu, Y., Springston, S. R., Souza, R.,](#)
1422 [Newburn, M. K., Alexander, M. L., Martin, S. T. and Jimenez, J. L.: Secondary organic aerosol](#)
1423 [formation from ambient air in an oxidation flow reactor in central Amazonia, Atmospheric Chem.](#)
1424 [Phys., 18\(1\), 467–493, doi:10.5194/acp-18-467-2018, 2018.](#)

1425 [Paulson, S. E., Pandis, S. N., Baltensperger, U., Seinfeld, J. H., Flagan, R. C., Palen, E. J., Allen,](#)
1426 [D. T., Schaffner, C., Giger, W. and Portmann, A.: Characterization of photochemical aerosols from](#)
1427 [biogenic hydrocarbons, J. Aerosol Sci., 21, S245–S248, doi:10.1016/0021-8502\(90\)90230-U,](#)
1428 [1990.](#)

1429 [Peng, Z. and Jimenez, J. L.: Modeling of the chemistry in oxidation flow reactors with high initial](#)
1430 [NO, Atmospheric Chem. Phys., 17\(19\), 11991–12010, doi:10.5194/acp-17-11991-2017, 2017.](#)

1431 [Peng, Z., Day, D. A., Stark, H., Li, R., Lee-Taylor, J., Palm, B. B., Brune, W. H. and Jimenez, J.](#)
1432 [L.: HO_x radical chemistry in oxidation flow reactors with low-pressure mercury lamps](#)
1433 [systematically examined by modeling, Atmospheric Meas. Tech., 8\(11\), 4863–4890,](#)
1434 [doi:10.5194/amt-8-4863-2015, 2015.](#)

1435 [Peng, Z., Day, D. A., Ortega, A. M., Palm, B. B., Hu, W., Stark, H., Li, R., Tsigaridis, K., Brune,](#)
1436 [W. H. and Jimenez, J. L.: Non-OH chemistry in oxidation flow reactors for the study of](#)
1437 [atmospheric chemistry systematically examined by modeling, Atmospheric Chem. Phys., 16\(7\),](#)
1438 [4283–4305, doi:10.5194/acp-16-4283-2016, 2016.](#)

1439 [Peng, Z., Palm, B. B., Day, D. A., Talukdar, R. K., Hu, W., Lambe, A. T., Brune, W. H. and](#)
1440 [Jimenez, J. L.: Model Evaluation of New Techniques for Maintaining High-NO Conditions in](#)

1441 [Oxidation Flow Reactors for the Study of OH-Initiated Atmospheric Chemistry, ACS Earth Space](#)
1442 [Chem., doi:10.1021/acsearthspacechem.7b00070, 2017.](#)

1443 [Pereira, K. L., Hamilton, J. F., Rickard, A. R., Bloss, W. J., Alam, M. S., Camredon, M., Ward,](#)
1444 [M. W., Wyche, K. P., Muñoz, A., Vera, T., Vázquez, M., Borrás, E. and Ródenas, M.: Insights](#)
1445 [into the Formation and Evolution of Individual Compounds in the Particulate Phase during](#)
1446 [Aromatic Photo-Oxidation, Environ. Sci. Technol., 49\(22\), 13168–13178,](#)
1447 [doi:10.1021/acs.est.5b03377, 2015.](#)

1448 [Renbaum, L. H. and Smith, G. D.: Artifacts in measuring aerosol uptake kinetics: the roles of time,](#)
1449 [concentration and adsorption, Atmospheric Chem. Phys., 11\(14\), 6881–6893, doi:10.5194/acp-11-](#)
1450 [6881-2011, 2011.](#)

1451 [Rudich, Y., Donahue, N. M. and Mentel, T. F.: Aging of Organic Aerosol: Bridging the Gap](#)
1452 [Between Laboratory and Field Studies, Annu. Rev. Phys. Chem., 58\(1\), 321–352,](#)
1453 [doi:10.1146/annurev.physchem.58.032806.104432, 2007.](#)

1454 [Seinfeld, J. H. and Pandis, S. N.: Atmospheric chemistry and physics: from air pollution to climate](#)
1455 [change, 2nd ed., J. Wiley, Hoboken, N.J., 2006.](#)

1456 [Simonen, P., Saukko, E., Karjalainen, P., Timonen, H., Bloss, M., Aakko-Saksa, P., Rönkkö, T.,](#)
1457 [Keskinen, J. and Dal Maso, M.: A New Oxidation Flow Reactor for Measuring Secondary Aerosol](#)
1458 [Formation of Rapidly Changing Emission Sources, Atmospheric Meas. Tech. Discuss., 1–27,](#)
1459 [doi:10.5194/amt-2016-300, 2016.](#)

1460 [Slowik, J. G., Wong, J. P. S. and Abbatt, J. P. D.: Real-time, controlled OH-initiated oxidation of](#)
1461 [biogenic secondary organic aerosol, Atmospheric Chem. Phys. Discuss., 12\(3\), 8183–8224,](#)
1462 [doi:10.5194/acpd-12-8183-2012, 2012.](#)

1463 [Smith, J. D., Kroll, J. H., Cappa, C. D., Che, D. L., Liu, C. L., Ahmed, M., Leone, S. R., Worsnop,](#)
1464 [D. R. and Wilson, K. R.: The heterogeneous reaction of hydroxyl radicals with sub-micron](#)
1465 [squalane particles: a model system for understanding the oxidative aging of ambient aerosols,](#)
1466 [Atmospheric Chem. Phys., 9\(9\), 3209–3222, doi:10.5194/acp-9-3209-2009, 2009.](#)

1467 [Sun, Y.: Study on the Internal Effect of Inhibiting Gas and Solid Back-Mixing in Fluidized Beds,](#)
1468 [Masters, Tsinghua University, Beijing., 2010.](#)

1469 [Taylor, G.: Dispersion of Soluble Matter in Solvent Flowing Slowly through a Tube, Proc. R. Soc.](#)
1470 [Math. Phys. Eng. Sci., 219\(1137\), 186–203, doi:10.1098/rspa.1953.0139, 1953.](#)

1471 [Taylor, G.: Conditions under Which Dispersion of a Solute in a Stream of Solvent can be Used to](#)
1472 [Measure Molecular Diffusion, Proc. R. Soc. Math. Phys. Eng. Sci., 225\(1163\), 473–477,](#)
1473 [doi:10.1098/rspa.1954.0216, 1954a.](#)

1474 [Taylor, G. I.: Diffusion and Mass Transport in Tubes, Proc. Phys. Soc. Sect. B, 67\(12\), 857–869,](#)
1475 [doi:10.1088/0370-1301/67/12/301, 1954b.](#)

1476 [Turpin, B. J., Saxena, P. and Andrews, E.: Measuring and simulating particulate organics in the](#)
1477 [atmosphere: problems and prospects, Atmos. Environ., 34\(18\), 2983–3013, doi:10.1016/S1352-](#)
1478 [2310\(99\)00501-4, 2000.](#)

1479 [Villermaux, J.: Macro and Micromixing Phenomena in Chemical Reactors, in Chemical Reactor](#)
1480 [Design and Technology, edited by H. I. Lasa, pp. 191–244, Springer Netherlands, Dordrecht.](#)
1481 [\[online\] Available from: \[http://www.springerlink.com/index/10.1007/978-94-009-4400-8_6\]\(http://www.springerlink.com/index/10.1007/978-94-009-4400-8_6\)](#)
1482 [\(Accessed 11 December 2015\), 1986.](#)

1483 [Volkamer, R., Platt, U. and Wirtz, K.: Primary and Secondary Glyoxal Formation from Aromatics:](#)
1484 [Experimental Evidence for the Bicycloalkyl–Radical Pathway from Benzene, Toluene, and *p* -](#)
1485 [Xylene, J. Phys. Chem. A, 105\(33\), 7865–7874, doi:10.1021/jp010152w, 2001.](#)

1486 [Went, F. W.: Blue Hazes in the Atmosphere, Nature, 187\(4738\), 641–643, doi:10.1038/187641a0,](#)
1487 [1960.](#)

1488 [Williams, B. J., Goldstein, A. H., Kreisberg, N. M. and Hering, S. V.: An In-Situ Instrument for](#)
1489 [Speciated Organic Composition of Atmospheric Aerosols: Thermal Desorption Aerosol GC/MS-](#)
1490 [FID \(TAG\), Aerosol Sci. Technol., 40\(8\), 627–638, doi:10.1080/02786820600754631, 2006.](#)

1491 [Zhao, Y., Kreisberg, N. M., Worton, D. R., Teng, A. P., Hering, S. V. and Goldstein, A. H.:](#)
1492 [Development of an *In Situ* Thermal Desorption Gas Chromatography Instrument for Quantifying](#)
1493 [Atmospheric Semi-Volatile Organic Compounds, Aerosol Sci. Technol., 47\(3\), 258–266,](#)
1494 [doi:10.1080/02786826.2012.747673, 2013.](#)

1495 [Zwietering, T. N.: The degree of mixing in continuous flow systems, Chem. Eng. Sci., 11\(1\), 1–](#)
1496 [15, doi:10.1016/0009-2509\(59\)80068-3, 1959.](#)

1497 [Aris, R.: On the Dispersion of a Solute in a Fluid Flowing through a Tube, Proc. R. Soc. Math.](#)
1498 [Phys. Eng. Sci., 235\(1200\), 67–77, doi:10.1098/rspa.1956.0065, 1956.](#)

1499 [Bourne, J. R.: Mixing and the Selectivity of Chemical Reactions, Org. Process Res. Dev., 7\(4\),](#)
1500 [471–508, doi:10.1021/op020074q, 2003.](#)

1501 [Brune, W. H., Schwab, J. J. and Anderson, J. G.: Laser magnetic resonance, resonance](#)
1502 [fluorescence, resonance absorption studies of the reaction kinetics of \$O + OH \rightarrow H + O_2\$, \$O + HO_2\$](#)
1503 [\$\rightarrow OH + O_2\$, \$N + OH \rightarrow H + NO\$, \$N + HO_2 \rightarrow\$ products at 300 K between 1 and 5 torr, J. Phys.](#)
1504 [Chem., 87\(22\), 4503–4514, doi:10.1021/j100245a034, 1983.](#)

1505 [Bruns, E. A., El Haddad, I., Keller, A., Klein, F., Kumar, N. K., Pieber, S. M., Corbin, J. C.,](#)
1506 [Slowik, J. G., Brune, W. H., Baltensperger, U. and Prévôt, A. S. H.: Inter-comparison of laboratory](#)
1507 [smog chamber and flow reactor systems on organic aerosol yield and composition, Atmospheric](#)
1508 [Meas. Tech., 8\(6\), 2315–2332, doi:10.5194/amt-8-2315-2015, 2015.](#)

1509 [Canagaratna, M. R., Jayne, J. T., Jimenez, J. L., Allan, J. D., Alfarra, M. R., Zhang, Q., Onasch,](#)
1510 [T. B., Drewnick, F., Coe, H., Middlebrook, A., Delia, A., Williams, L. R., Trimborn, A. M.,](#)
1511 [Northway, M. J., DeCarlo, P. F., Kolb, C. E., Davidovits, P. and Worsnop, D. R.: Chemical and](#)

1512 microphysical characterization of ambient aerosols with the aerodyne aerosol mass spectrometer,
1513 *Mass Spectrom. Rev.*, 26(2), 185–222, doi:10.1002/mas.20115, 2007.

1514 Cazorla, M. and Brune, W. H.: Measurement of Ozone Production Sensor, *Atmospheric Meas.*
1515 *Tech.*, 3(3), 545–555, doi:10.5194/amt-3-545-2010, 2010.

1516 Chhabra, P. S., Lambe, A. T., Canagaratna, M. R., Stark, H., Jayne, J. T., Onasch, T. B.,
1517 Davidovits, P., Kimmel, J. R. and Worsnop, D. R.: Application of high-resolution time-of-flight
1518 chemical ionization mass spectrometry measurements to estimate volatility distributions of α -
1519 pinene and naphthalene oxidation products, *Atmospheric Meas. Tech.*, 8(1), 1–18,
1520 doi:10.5194/amt-8-1-2015, 2015.

1521 Claeys, M.: Formation of Secondary Organic Aerosols Through Photooxidation of Isoprene,
1522 *Science*, 303(5661), 1173–1176, doi:10.1126/science.1092805, 2004.

1523 Crouse, J. D., McKinney, K. A., Kwan, A. J. and Wennberg, P. O.: Measurement of Gas Phase
1524 Hydroperoxides by Chemical Ionization Mass Spectrometry, *Anal. Chem.*, 78(19), 6726–6732,
1525 doi:10.1021/ac0604235, 2006.

1526 Crump, J. G. and Seinfeld, J. H.: Aerosol behavior in the continuous stirred tank reactor, *AIChE*
1527 *J.*, 26(4), 610–616, doi:10.1002/aic.690260412, 1980.

1528 Crump, J. G., Flagan, R. C. and Seinfeld, J. H.: Particle Wall Loss Rates in Vessels, *Aerosol Sci.*
1529 *Technol.*, 2(3), 303–309, doi:10.1080/02786828308958636, 1982.

1530 Danckwerts, P. V.: Continuous flow systems, *Chem. Eng. Sci.*, 2(1), 1–13, doi:10.1016/0009-
1531 2509(53)80001-1, 1953.

1532 Deckwer, W. D.: Non-isobaric bubble columns with variable gas velocity, *Chem. Eng. Sci.*, 31(4),
1533 309–317, doi:10.1016/0009-2509(76)85076-2, 1976.

1534 Ezell, M. J., Johnson, S. N., Yu, Y., Perraud, V., Bruns, E. A., Alexander, M. L., Zelenyuk, A.,
1535 Dabdub, D. and Finlayson Pitts, B. J.: A New Aerosol Flow System for Photochemical and
1536 Thermal Studies of Tropospheric Aerosols, *Aerosol Sci. Technol.*, 44(5), 329–338,
1537 doi:10.1080/02786821003639700, 2010.

1538 Fogler, H. S.: Elements of chemical reaction engineering, 4th ed., Prentice Hall PTR, Upper Saddle
1539 River, NJ., 2006.

1540 George, I. J. and Abbatt, J. P. D.: Chemical evolution of secondary organic aerosol from OH-
1541 initiated heterogeneous oxidation, *Atmospheric Chem. Phys.*, 10(12), 5551–5563,
1542 doi:10.5194/acp-10-5551-2010, 2010.

1543 George, I. J., Vlasenko, A., Slowik, J. G., Broekhuizen, K. and Abbatt, J. P. D.: Heterogeneous
1544 oxidation of saturated organic aerosols by hydroxyl radicals: uptake kinetics, condensed phase
1545 products, and particle size change, *Atmospheric Chem. Phys.*, 7(16), 4187–4201, doi:10.5194/acp-
1546 7-4187-2007, 2007.

1547 de Gouw, J. and Warneke, C.: Measurements of volatile organic compounds in the earth's
1548 atmosphere using proton transfer reaction mass spectrometry, *Mass Spectrom. Rev.*, 26(2), 223–
1549 257, doi:10.1002/mas.20119, 2007.

1550 Haagen-Smit, A. J.: Chemistry and Physiology of Los Angeles Smog, *Ind. Eng. Chem.*, 44(6),
1551 1342–1346, doi:10.1021/ie50510a045, 1952.

1552 Haagen-Smit, A. J.: Photochemistry and Smog, *J. Air Pollut. Control Assoc.*, 13(9), 444–454,
1553 doi:10.1080/00022470.1963.10468205, 1963.

1554 Haagen-Smit, A. J.: A Lesson from the Smog Capital of the World, *Proc. Natl. Acad. Sci.*, 67(2),
1555 887–897, doi:10.1073/pnas.67.2.887, 1970.

1556 Hamed, M.: Hydrodynamics, Mixing, and Mass Transfer in Bubble Columns with Internals, PhD,
1557 Washington University in St. Louis, Saint Louis., 2012.

1558 Han, L.: Hydrodynamics, back-mixing, and mass transfer in a slurry bubble column reactor for
1559 Fischer-Tropsch alternative fuels, DSc, Washington University in St. Louis, Saint Louis., 2007.

1560 Hansel, A., Jordan, A., Holzinger, R., Prazeller, P., Vogel, W. and Lindinger, W.: Proton transfer
1561 reaction mass spectrometry: on-line trace gas analysis at the ppb level, *Int. J. Mass Spectrom. Ion
1562 Process.*, 149–150, 609–619, doi:10.1016/0168-1176(95)04294-U, 1995.

1563 Howard, C. J.: Kinetic measurements using flow tubes, *J. Phys. Chem.*, 83(1), 3–9,
1564 doi:10.1021/j100464a001, 1979.

1565 Huang, Y., Coggon, M. M., Zhao, R., Lignell, H., Bauer, M. U., Flagan, R. C. and Seinfeld, J. H.:
1566 The Caltech Photooxidation Flow Tube Reactor – I: Design and Fluid Dynamics,
1567 *Atmospheric Meas. Tech. Discuss.*, 1–36, doi:10.5194/amt-2016-282, 2016.

1568 Jayne, J. T., Leard, D. C., Zhang, X., Davidovits, P., Smith, K. A., Kolb, C. E. and Worsnop, D.
1569 R.: Development of an Aerosol Mass Spectrometer for Size and Composition Analysis of
1570 Submicron Particles, *Aerosol Sci. Technol.*, 33(1–2), 49–70, doi:10.1080/027868200410840,
1571 2000.

1572 Kamens, R. M., Gery, M. W., Jeffries, H. E., Jackson, M. and Cole, E. I.: Ozone-isoprene
1573 reactions: Product formation and aerosol potential, *Int. J. Chem. Kinet.*, 14(9), 955–975,
1574 doi:10.1002/kin.550140902, 1982.

1575 Kang, E., Root, M. J., Toohey, D. W. and Brune, W. H.: Introducing the concept of Potential
1576 Aerosol Mass (PAM), *Atmospheric Chem. Phys.*, 7(22), 5727–5744, doi:10.5194/acp-7-5727-
1577 2007, 2007.

1578 Kang, E., Toohey, D. W. and Brune, W. H.: Dependence of SOA oxidation on organic aerosol
1579 mass concentration and OH exposure: experimental PAM chamber studies, *Atmospheric Chem.
1580 Phys.*, 11(4), 1837–1852, doi:10.5194/acp-11-1837-2011, 2011.

1581 Katrib, Y., Biskos, G., Buseck, P. R., Davidovits, P., Jayne, J. T., Mochida, M., Wise, M. E.,
1582 Worsnop, D. R. and Martin, S. T.: Ozonolysis of Mixed Oleic Acid/Stearic Acid Particles:
1583 Reaction Kinetics and Chemical Morphology, *J. Phys. Chem. A*, 109(48), 10910–10919,
1584 doi:10.1021/jp054714d, 2005.

1585 Keller, A. and Burtscher, H.: A continuous photo-oxidation flow reactor for a defined
1586 measurement of the SOA formation potential of wood burning emissions, *J. Aerosol Sci.*, 49, 9–
1587 20, doi:10.1016/j.jaerosci.2012.02.007, 2012.

1588 Kessler, S. H., Smith, J. D., Che, D. L., Worsnop, D. R., Wilson, K. R. and Kroll, J. H.: Chemical
1589 Sinks of Organic Aerosol: Kinetics and Products of the Heterogeneous Oxidation of Erythritol and
1590 Levoglucosan, *Environ. Sci. Technol.*, 44(18), 7005–7010, doi:10.1021/es101465m, 2010.

1591 Kessler, S. H., Nah, T., Daumit, K. E., Smith, J. D., Leone, S. R., Kolb, C. E., Worsnop, D. R.,
1592 Wilson, K. R. and Kroll, J. H.: OH-Initiated Heterogeneous Aging of Highly Oxidized Organic
1593 Aerosol, *J. Phys. Chem. A*, 116(24), 6358–6365, doi:10.1021/jp212131m, 2012.

1594 Keyser, L. F.: Absolute rate constant of the reaction $\text{OH} + \text{H}_2\text{O}_2 \rightarrow \text{HO}_2 + \text{H}_2\text{O}$ from 245 to 423
1595 K, *J. Phys. Chem.*, 84(13), 1659–1663, doi:10.1021/j100450a001, 1980.

1596 Keyser, L. F.: High-pressure flow kinetics. A study of the hydroxyl + hydrogen chloride reaction
1597 from 2 to 100 torr, *J. Phys. Chem.*, 88(20), 4750–4758, doi:10.1021/j150664a061, 1984.

1598 Knopf, D. A., Anthony, L. M. and Bertram, A. K.: Reactive Uptake of O_3 by Multicomponent and
1599 Multiphase Mixtures Containing Oleic Acid, *J. Phys. Chem. A*, 109(25), 5579–5589,
1600 doi:10.1021/jp0512513, 2005.

1601 Kroll, J. H. and Seinfeld, J. H.: Chemistry of secondary organic aerosol: Formation and evolution
1602 of low volatility organics in the atmosphere, *Atmos. Environ.*, 42(16), 3593–3624,
1603 doi:10.1016/j.atmosenv.2008.01.003, 2008.

1604 Kroll, J. H., Ng, N. L., Murphy, S. M., Flagan, R. C. and Seinfeld, J. H.: Secondary Organic
1605 Aerosol Formation from Isoprene Photooxidation, *Environ. Sci. Technol.*, 40(6), 1869–1877,
1606 doi:10.1021/es0524301, 2006.

1607 Kroll, J. H., Smith, J. D., Worsnop, D. R. and Wilson, K. R.: Characterisation of lightly oxidised
1608 organic aerosol formed from the photochemical aging of diesel exhaust particles, *Environ. Chem.*,
1609 9(3), 211, doi:10.1071/EN11162, 2012.

1610 Lamb, J. J., Molina, L. T., Smith, C. A. and Molina, M. J.: Rate constant of the hydroxy radical +
1611 hydrogen peroxide \rightarrow hydroperoxy radical + water reaction, *J. Phys. Chem.*, 87(22), 4467–
1612 4470, doi:10.1021/j100245a028, 1983.

1613 Lambe, A. T., Ahern, A. T., Williams, L. R., Slowik, J. G., Wong, J. P. S., Abbatt, J. P. D., Brune,
1614 W. H., Ng, N. L., Wright, J. P., Croasdale, D. R., Worsnop, D. R., Davidovits, P. and Onasch, T.
1615 B.: Characterization of aerosol photooxidation flow reactors: heterogeneous oxidation, secondary
1616 organic aerosol formation and cloud condensation nuclei activity measurements, *Atmospheric*
1617 *Meas. Tech.*, 4(3), 445–461, doi:10.5194/amt-4-445-2011, 2011a.

1618 Lambe, A. T., Onasch, T. B., Massoli, P., Croasdale, D. R., Wright, J. P., Ahern, A. T., Williams,
1619 L. R., Worsnop, D. R., Brune, W. H. and Davidovits, P.: Laboratory studies of the chemical
1620 composition and cloud condensation nuclei (CCN) activity of secondary organic aerosol (SOA)
1621 and oxidized primary organic aerosol (OPOA), *Atmospheric Chem. Phys. Discuss.*, 11(5), 13617–
1622 13653, doi:10.5194/acpd-11-13617-2011, 2011b.

1623 Lambe, A. T., Onasch, T. B., Croasdale, D. R., Wright, J. P., Martin, A. T., Franklin, J. P., Massoli,
1624 P., Kroll, J. H., Canagaratna, M. R., Brune, W. H., Worsnop, D. R. and Davidovits, P.: Transitions
1625 from Functionalization to Fragmentation Reactions of Laboratory Secondary Organic Aerosol
1626 (SOA) Generated from the OH Oxidation of Alkane Precursors, *Environ. Sci. Technol.*, 46(10),
1627 5430–5437, doi:10.1021/es300274t, 2012.

1628 Lambe, A. T., Cappa, C. D., Massoli, P., Onasch, T. B., Forestieri, S. D., Martin, A. T., Cummings,
1629 M. J., Croasdale, D. R., Brune, W. H., Worsnop, D. R. and Davidovits, P.: Relationship between
1630 Oxidation Level and Optical Properties of Secondary Organic Aerosol, *Environ. Sci. Technol.*,
1631 130606090408002, doi:10.1021/es401043j, 2013.

1632 Lambe, A. T., Chhabra, P. S., Onasch, T. B., Brune, W. H., Hunter, J. F., Kroll, J. H., Cummings,
1633 M. J., Brogan, J. F., Parmar, Y., Worsnop, D. R., Kolb, C. E. and Davidovits, P.: Effect of oxidant
1634 concentration, exposure time, and seed particles on secondary organic aerosol chemical
1635 composition and yield, *Atmospheric Chem. Phys.*, 15(6), 3063–3075, doi:10.5194/acp-15-3063-
1636 2015, 2015.

1637 Leone, J. A., Flagan, R. C., Grosjean, D. and Seinfeld, J. H.: An outdoor smog chamber and
1638 modeling study of toluene-NO_x photooxidation, *Int. J. Chem. Kinet.*, 17(2), 177–216,
1639 doi:10.1002/kin.550170206, 1985.

1640 Levenspiel, O.: *Chemical reaction engineering*, 3rd ed., Wiley, New York., 1999.

1641 Levenspiel, O.: *The chemical reactor omnibook*, OSU Book Stores, Corvallis, Or., 2002.

1642 Li, R., Palm, B. B., Ortega, A. M., Hlywiak, J., Hu, W., Peng, Z., Day, D. A., Knote, C., Brune,
1643 W. H., de Gouw, J. A. and Jimenez, J. L.: Modeling the Radical Chemistry in an Oxidation Flow
1644 Reactor: Radical Formation and Recycling, Sensitivities, and the OH Exposure Estimation
1645 Equation, *J. Phys. Chem. A*, 119(19), 4418–4432, doi:10.1021/jp509534k, 2015.

1646 Liu, P. F., Abdelmalki, N., Hung, H. M., Wang, Y., Brune, W. H. and Martin, S. T.: Ultraviolet
1647 and visible complex refractive indices of secondary organic material produced by photooxidation
1648 of the aromatic compounds toluene and m-xylene, *Atmospheric Chem. Phys.*, 15(3), 1435–1446,
1649 doi:10.5194/acp-15-1435-2015, 2015.

1650 MacMullin, R. B. and Weber Jr., M.: The theory of short-circuiting in continuous-flow mixing
1651 vessels in series and the kinetics of chemical reactions in such systems, *Trans. Am. Inst. Chem.*
1652 *Eng.*, 31, 409–458, 1935.

1653 Massoli, P., Lambe, A. T., Ahern, A. T., Williams, L. R., Ehn, M., Mikkilä, J., Canagaratna, M.
1654 R., Brune, W. H., Onasch, T. B., Jayne, J. T., Petäjä, T., Kulmala, M., Laaksonen, A., Kolb, C. E.,
1655 Davidovits, P. and Worsnop, D. R.: Relationship between aerosol oxidation level and hygroscopic

1656 properties of laboratory generated secondary organic aerosol (SOA) particles:
1657 ~~HYGROSCOPICITY OF LABORATORY SOA~~, *Geophys. Res. Lett.*, 37(24), n/a n/a,
1658 doi:10.1029/2010GL045258, 2010.

1659 McNeill, V. F., Yatavelli, R. L. N., Thornton, J. A., Stipe, C. B. and Landgrebe, O.: Heterogeneous
1660 OH oxidation of palmitic acid in single component and internally mixed aerosol particles:
1661 vaporization and the role of particle phase, *Atmospheric Chem. Phys.*, 8(17), 5465–5476,
1662 doi:10.5194/acp-8-5465-2008, 2008.

1663 Mills, P. L. and Duduković, M. P.: Deconvolution of noisy tracer response data by a linear filtering
1664 method, *AIChE J.*, 34(10), 1752–1756, doi:10.1002/aic.690341025, 1988.

1665 Nozière, B., Barnes, I. and Becker, K. H.: Product study and mechanisms of the reactions of α -
1666 pinene and of pinonaldehyde with OH radicals, *J. Geophys. Res.*, 104(D19), 23645,
1667 doi:10.1029/1999JD900778, 1999.

1668 Ortega, A. M., Day, D. A., Cubison, M. J., Brune, W. H., Bon, D., de Gouw, J. A. and Jimenez, J.
1669 L.: Secondary organic aerosol formation and primary organic aerosol oxidation from biomass-
1670 burning smoke in a flow reactor during FLAME 3, *Atmospheric Chem. Phys.*, 13(22), 11551–
1671 11571, doi:10.5194/acp-13-11551-2013, 2013.

1672 Ortega, A. M., Hayes, P. L., Peng, Z., Palm, B. B., Hu, W., Day, D. A., Li, R., Cubison, M. J.,
1673 Brune, W. H., Graus, M., Warneke, C., Gilman, J. B., Kuster, W. C., de Gouw, J. A. and Jimenez,
1674 J. L.: Real time measurements of secondary organic aerosol formation and aging from ambient air
1675 in an oxidation flow reactor in the Los Angeles area, *Atmospheric Chem. Phys. Discuss.*, 15(15),
1676 21907–21958, doi:10.5194/acpd-15-21907-2015, 2015.

1677 Paulson, S. E., Pandis, S. N., Baltensperger, U., Seinfeld, J. H., Flagan, R. C., Palen, E. J., Allen,
1678 D. T., Schaffner, C., Giger, W. and Portmann, A.: Characterization of photochemical aerosols from
1679 biogenic hydrocarbons, *J. Aerosol Sci.*, 21, S245–S248, doi:10.1016/0021-8502(90)90230-U,
1680 1990.

1681 Peng, Z., Day, D. A., Stark, H., Li, R., Lee-Taylor, J., Palm, B. B., Brune, W. H. and Jimenez, J.
1682 L.: HO_x radical chemistry in oxidation flow reactors with low pressure mercury lamps
1683 systematically examined by modeling, *Atmospheric Meas. Tech.*, 8(11), 4863–4890,
1684 doi:10.5194/amt-8-4863-2015, 2015.

1685 Peng, Z., Day, D. A., Ortega, A. M., Palm, B. B., Hu, W., Stark, H., Li, R., Tsigaridis, K., Brune,
1686 W. H. and Jimenez, J. L.: Non-OH chemistry in oxidation flow reactors for the study of
1687 atmospheric chemistry systematically examined by modeling, *Atmospheric Chem. Phys.*, 16(7),
1688 4283–4305, doi:10.5194/acp-16-4283-2016, 2016.

1689 Pereira, K. L., Hamilton, J. F., Rickard, A. R., Bloss, W. J., Alam, M. S., Camredon, M., Ward,
1690 M. W., Wyche, K. P., Muñoz, A., Vera, T., Vázquez, M., Borrás, E. and Ródenas, M.: Insights
1691 into the Formation and Evolution of Individual Compounds in the Particulate Phase during
1692 Aromatic Photo-Oxidation, *Environ. Sci. Technol.*, 49(22), 13168–13178,
1693 doi:10.1021/acs.est.5b03377, 2015.

1694 Renbaum, L. H. and Smith, G. D.: Artifacts in measuring aerosol uptake kinetics: the roles of time,
1695 concentration and adsorption, *Atmospheric Chem. Phys.*, 11(14), 6881–6893, doi:10.5194/acp-11-
1696 6881-2011, 2011.

1697 Rudich, Y., Donahue, N. M. and Mentel, T. F.: Aging of Organic Aerosol: Bridging the Gap
1698 Between Laboratory and Field Studies, *Annu. Rev. Phys. Chem.*, 58(1), 321–352,
1699 doi:10.1146/annurev.phychem.58.032806.104432, 2007.

1700 Seinfeld, J. H. and Pandis, S. N.: Atmospheric chemistry and physics: from air pollution to climate
1701 change, 2nd ed., J. Wiley, Hoboken, N.J., 2006.

1702 Simonen, P., Saukko, E., Karjalainen, P., Timonen, H., Bloss, M., Aakko-Saksa, P., Rönkkö, T.,
1703 Keskinen, J. and Dal Maso, M.: A New Oxidation Flow Reactor for Measuring Secondary Aerosol
1704 Formation of Rapidly Changing Emission Sources, *Atmospheric Meas. Tech. Discuss.*, 1–27,
1705 doi:10.5194/amt-2016-300, 2016.

1706 Slowik, J. G., Wong, J. P. S. and Abbatt, J. P. D.: Real-time, controlled OH-initiated oxidation of
1707 biogenic secondary organic aerosol, *Atmospheric Chem. Phys. Discuss.*, 12(3), 8183–8224,
1708 doi:10.5194/acpd-12-8183-2012, 2012.

1709 Smith, J. D., Kroll, J. H., Cappa, C. D., Che, D. L., Liu, C. L., Ahmed, M., Leone, S. R., Worsnop,
1710 D. R. and Wilson, K. R.: The heterogeneous reaction of hydroxyl radicals with sub-micron
1711 squalane particles: a model system for understanding the oxidative aging of ambient aerosols,
1712 *Atmospheric Chem. Phys.*, 9(9), 3209–3222, doi:10.5194/acp-9-3209-2009, 2009.

1713 Sun, Y.: Study on the Internal Effect of Inhibiting Gas and Solid Back-Mixing in Fluidized Beds,
1714 Masters, Tsinghua University, Beijing., 2010.

1715 Taylor, G.: Dispersion of Soluble Matter in Solvent Flowing Slowly through a Tube, *Proc. R. Soc.*
1716 *Math. Phys. Eng. Sci.*, 219(1137), 186–203, doi:10.1098/rspa.1953.0139, 1953.

1717 Taylor, G.: Conditions under Which Dispersion of a Solute in a Stream of Solvent can be Used to
1718 Measure Molecular Diffusion, *Proc. R. Soc. Math. Phys. Eng. Sci.*, 225(1163), 473–477,
1719 doi:10.1098/rspa.1954.0216, 1954a.

1720 Taylor, G. I.: Diffusion and Mass Transport in Tubes, *Proc. Phys. Soc. Sect. B*, 67(12), 857–869,
1721 doi:10.1088/0370-1301/67/12/301, 1954b.

1722 Turpin, B. J., Saxena, P. and Andrews, E.: Measuring and simulating particulate organics in the
1723 atmosphere: problems and prospects, *Atmos. Environ.*, 34(18), 2983–3013, doi:10.1016/S1352-
1724 2310(99)00501-4, 2000.

1725 Villermaux, J.: Macro and Micromixing Phenomena in Chemical Reactors, in *Chemical Reactor*
1726 *Design and Technology*, edited by H. I. Lasa, pp. 191–244, Springer Netherlands, Dordrecht.
1727 [online] Available from: http://www.springerlink.com/index/10.1007/978-94-009-4400-8_6
1728 (Accessed 11 December 2015), 1986.

1729 Volkamer, R., Platt, U. and Wirtz, K.: Primary and Secondary Glyoxal Formation from Aromatics:
1730 Experimental Evidence for the Bicycloalkyl Radical Pathway from Benzene, Toluene, and *p*-
1731 Xylene, *J. Phys. Chem. A*, 105(33), 7865–7874, doi:10.1021/jp010152w, 2001.

1732 Went, F. W.: Blue Hazes in the Atmosphere, *Nature*, 187(4738), 641–643, doi:10.1038/187641a0,
1733 1960.

1734 Williams, B. J., Goldstein, A. H., Kreisberg, N. M. and Hering, S. V.: An In-Situ Instrument for
1735 Speciated Organic Composition of Atmospheric Aerosols: Thermal Desorption Aerosol GC/MS-
1736 FID (TAG), *Aerosol Sci. Technol.*, 40(8), 627–638, doi:10.1080/02786820600754631, 2006.

1737 Zhao, Y., Kreisberg, N. M., Worton, D. R., Teng, A. P., Hering, S. V. and Goldstein, A. H.:
1738 Development of an *In Situ* Thermal Desorption Gas Chromatography Instrument for Quantifying
1739 Atmospheric Semi-Volatile Organic Compounds, *Aerosol Sci. Technol.*, 47(3), 258–266,
1740 doi:10.1080/02786826.2012.747673, 2013.

1741 Zwietering, T. N.: The degree of mixing in continuous flow systems, *Chem. Eng. Sci.*, 11(1), 1–
1742 15, doi:10.1016/0009-2509(59)80068-3, 1959.

1743

1744

1745

1746

1747